Chapter 4

THE GEOMAGNETIC FIELD

D.J. Knecht and B.M. Shuman

The existence of the geomagnetic field has been recognized for a very long time. The usefulness of a magnet as a directional reference was probably known in China more than 1000 years ago and in Europe at least 800 years ago. As early as the 15th century, the earlier belief that a compass needle points true north was found to be incorrect and mariners and mapmakers took account of this. Recorded measurements of the magnetic declination (the deviation of the compass from true north) at various locations on the earth date back to the early 16th century, which also saw the discovery of the magnetic dip (the deviation of a compass needle from horizontal when unconstrained). Although experiments with magnets had been carried out since the 13th century, the concept that the earth itself is a magnet was not advanced until the end of the 16th century by Gilbert.

From these beginnings, geomagnetism as a branch of science was developed. It was first assumed that the magnetism of the earth was like that of a solid permanent magnet and was therefore expected to be constant in the absence of major geological changes, but this view was soon proved wrong; the secular variation (changes in the field over time intervals of years or centuries) was discovered in the 17th century. Transient variations of the field (geomagnetic disturbance) were observed during the 18th century, and geomagnetism was increasingly appreciated to be a dynamic phenomenon.

By the early 19th century, a large number of magnetic observatories had been established both in European countries and in the distant lands of their empires. Through coordinated measurements by many stations, the geographic dependence of some geomagnetic phenomena was discovered and the worldwide nature of major disturbances was established. The increasing volume and precision of accumulated data made discouragingly clear how complex were the phenomena being studied. Increasing international cooperation included investigations during the first International Polar Year (1882–1883). By this time, the correlation between the 11-year periodicities of sunspot occurrence and geomagnetic phenomena had been noted. Early in the 20th century the intimate connection between solar and geomagnetic phenomena was further established by the correlation of recurrent disturbances with the 27-day solar rotation and later by the correlation of magnetic storms with solar flares.

However, the most important connection, the fact that the geomagnetic field interacts with a continuous stream of solar plasma, was established only within the last twenty years. As a result of satellite investigations, these recent years have seen drastic revisions in many fundamental ideas concerning the configuration of current systems and the magnetic field above the surface of the earth.

But while satellite measurements have expanded our understanding of the space above us, the development of techniques for collecting and interpreting archaeological and geological data have led to some important discoveries about the earth below us: namely, that the continents have drifted thousands of miles from their original locations and that the entire geomagnetic field undergoes periodic reversals.

Today, geomagnetism encompasses two broad areas of theoretical study that are served by overlapping experimental data bases: the physics of the interior of the earth (which produces the steady and slowly varying field) and the physics of the magnetosphere and ionosphere (which produce the dynamic behavior of the field). The material in this chapter tends to neglect the physics in favor of a description of geomagnetic phenomena and their experimental observation, but this neglect is partly remedied in other chapters on the ionosphere and magnetosphere.

4.1 BASIC CONCEPTS

4.1.1 Units, Terminology, and Conventions

The geomagnetic field is characterized at any point by its direction and magnitude, which can be specified by two direction angles and the magnitude, the magnitude of three perpendicular components, or some other set of three independent parameters. Angles are commonly measured in degrees, minutes, and seconds. Prior to widespread adoption of mks units, the magnitude was usually given in units of oersted (magnetic intensity) or gauss (magnetic induction). Since the field is less than one oersted everywhere, the unit gamma was most useful; one gamma equals 10^{-5} oersted or 10^{-5} gauss and was used interchangeably for intensity and induction. Since the mks unit for field strength is very large

(one tesla = 10^4 gauss), the nanotesla (nT), which very conveniently equals one gamma, is now almost universally used.

Some of the angles and components commonly employed are shown in Figure 4-1. Standard terminology is as follows. The vector geomagnetic field is the vector **F**. Its magnitude F is called the total intensity or the total field.

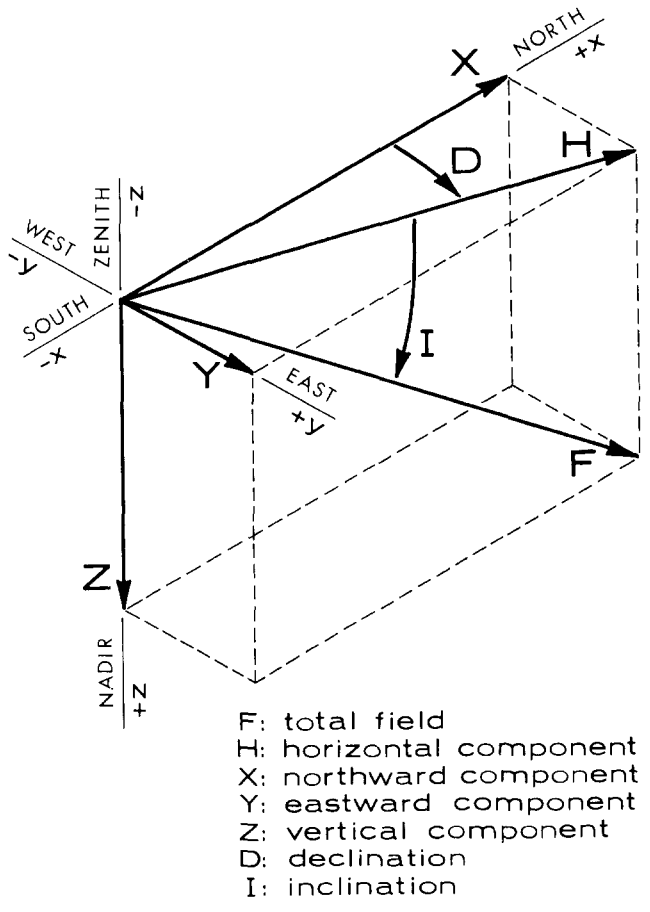

Figure 4-1. Definition and sign convention for the magnetic elements.

The magnitude H of the horizontal component vector **H** is called the horizontal intensity; the magnitude Z of the vertical component vector **Z** is called the vertical intensity. The northward, eastward, and downward components of the field are designated by the magnitudes X, Y, and Z, respectively, the Cartesian components of the field. The magnitude D of the angle between X and H is called the declination, the magnetic variation, or the variation of the compass. The magnitude I of the angle between **H** or **F** is called the inclination or the dip. The quantities F, H, X, Y, Z, D and I are called magnetic elements. The sets of elements used most commonly to specify the field are (H, D, Z); (F, I, D); and (X, Y, Z). The sign convention for each parameter is shown in the figure, all vectors and angles being positive as drawn.

4.1.2 Coordinate Systems

A number of coordinate systems are employed in the description of geomagnetic phenomena. Five of the most useful are the geographic, geomagnetic, geocentric solar-ecliptic, geocentric solar-magnetospheric, and solar-magnetic systems. They are shown in Figure 4-2 and are defined as follows.

A geographic coordinate system is one that is fixed with respect to the rotating earth and aligned with the axis of rotation. Most commonly used are the spherical polar coordinates r, θ, and φ, where r is geocentric distance, θ is colatitude (measured from the north geographic pole), and

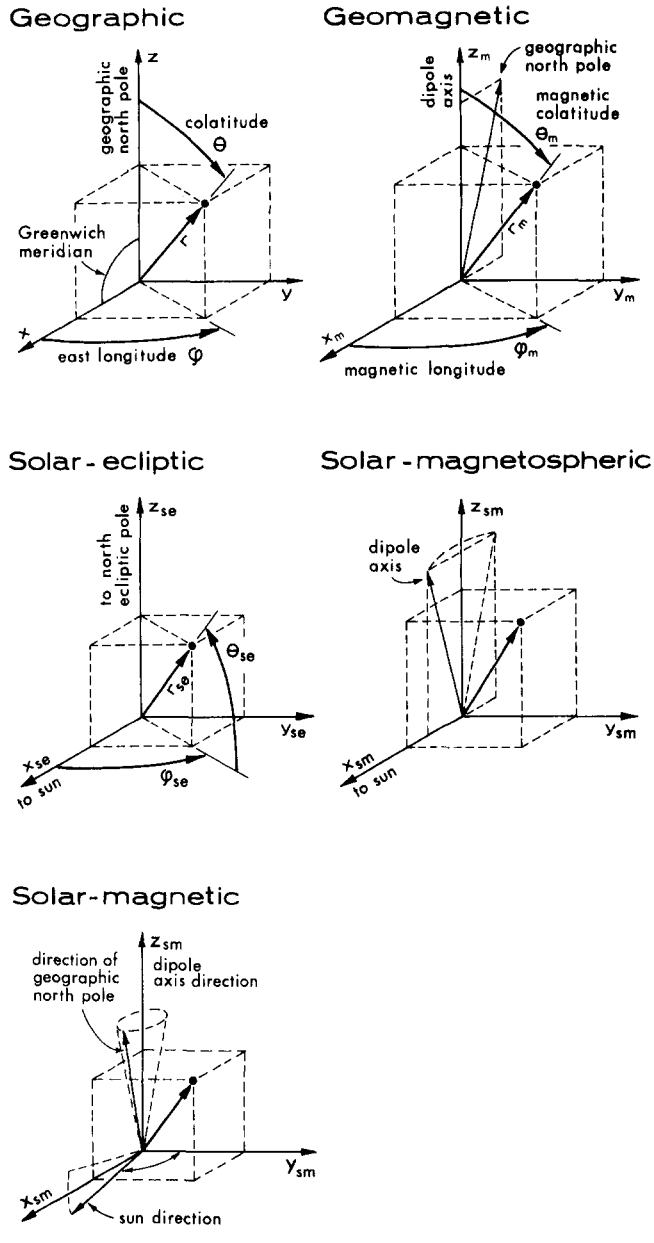

Figure 4-2. Several coordinate systems used in geomagnetism.

ϕ is east longitude (measured from the Greenwich meridian), with the earth assumed spherical. Sometimes altitude (above the surface of the earth) is specified in place of r, north or south latitude is specified in place of θ, and west longitude is specified in place of ϕ for values greater than 180 degrees. (Geodetic coordinates, which are defined relative to the nonspherical earth ellipsoid, must be used with care.)

The geomagnetic coordinate system is also a spherical polar system fixed relative to the earth, but the polar axis is the axis inclined 11.5 degrees to the axis of rotation, intersecting the earth surface at the point 78.5°N, 291.0°E which defines the geomagnetic north pole. This was at one time the axis of the best centered-dipole approximation to the field; current spherical-harmonic models of the main field would place the pole approximately 0.25 degrees farther north and 1.6 degrees farther west. Geomagnetic coordinates r, θ_m, and ϕ_m (and geomagnetic latitude and longitude) are defined by analogy with geographic coordinates, with ϕ_m (or geomagnetic longitude) measured from the American half of the great circle which passes through both the geographic and geomagnetic poles (that is, the zero-degree geomagnetic meridian coincides with 291.0°E geographic longitude over most of its length).

The corrected geomagnetic coordinate system is a refinement (of the geomagnetic coordinate system) that has proved useful in considering phenomena that involve propagation along lines of force of the geomagnetic field [Hakura, 1965]. It effectively provides a more accurate field-line connection from a point on (or near) the earth surface either to the equatorial plane or to its conjugate point than would be afforded by any simple dipole approximation of the geomagnetic field. Figure 4-3 shows how the corrected geomagnetic coordinates (latitude Φ_c and longitude Λ_c) are obtained for a point Q, at the earth surface, whose geomagnetic coordinates are Φ and Λ. Starting at Q, an "actual" field line (that is, one computed from an accurate higher-order model fitted to the actual geomagnetic field, as described in Section 4.6.1) is traced out to intersect the magnetic equatorial plane at the point A, which has polar coordinates L_c and Λ_c. From here a simple dipole field line is projected back toward the earth to a "landing point" Q_c. The corrected coordinates for point Q are the uncorrected coordinates of point Q_c (Φ_c and Λ_c). The value of Φ_c may be found from the dipole equation, $L_c = R \sec^2 \Phi_c$, where R is the radius of the earth. Assigning the corrected coordinates to the point Q permits an accurate description of phenomena in the actual field as if it were a simple dipole field; for example, points having the same coordinates in the northern and southern hemispheres will be actual conjugate points. A revised tabulation of corrected geomagnetic coordinates, using terms through order 7 in the spherical-harmonic model, has been published by Gustafsson [1970] for every 5° of geographic longitude and every 2° of geographic latitude.

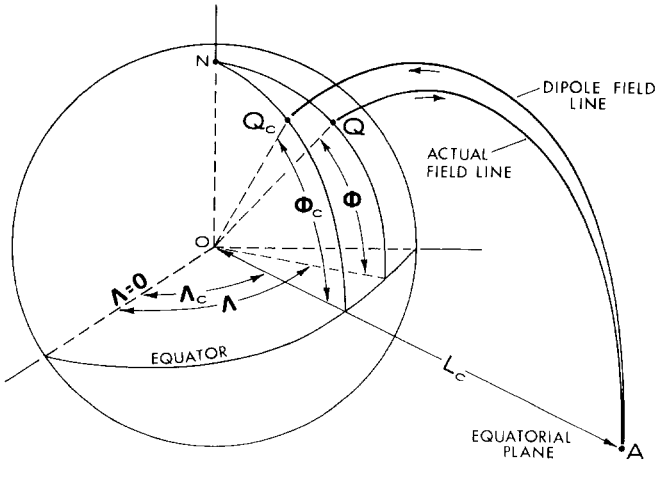

Figure 4-3. Method of finding corrected geomagnetic coordinates.

The geocentric solar-ecliptic (GSE) coordinate system is a right-handed Cartesian system with coordinates X_{se}, Y_{se}, and Z_{se}, and the center of the earth as origin. The positive X_{se} axis is directed toward the sun. The Z_{se} axis is directed toward the northern ecliptic pole, so both the X_{se} and Y_{se} axes lie in the ecliptic plane. This system therefore rotates slowly in space with the orbital period of the earth. In this system, field vectors are often resolved into two components, one lying in and the other perpendicular to the ecliptic plane; the direction of the former is specified by the angle ϕ between it and the X_{se} axis (positive counterclockwise when viewed from the northern pole). The direction of the total field is specified by ϕ and θ, where θ is the angle between the vector and the ecliptic plane (positive northward). This system is particularly useful for referencing data from interplanetary space, such as measurements of the undisturbed solar wind and the interplanetary magnetic field.

The geocentric solar magnetospheric (GSM) coordinate system is also a right-handed Cartesian system, with coordinates X_{sm}, Y_{sm}, and Z_{sm}, and its origin at the center of the earth. The positive X_{sm} axis is also directed toward the sun. It differs from the solar-ecliptic system in that the Z_{sm} axis lies in the plane containing both the X_{sm} axis and the geomagnetic dipole axis defined above. The system therefore not only rotates with the orbital period of the earth but also rocks back and forth through 23 degrees (a rotation about the X_{sm} axis) with a period of one day. This system is particularly useful for referencing data from distant regions of the magnetosphere, since time-dependent features that result from the conical motion of the dipole axis are, to a large extent, eliminated; that is, to a first approximation, the entire magnetosphere, in its main features, may be expected to rock back and forth in this way.

A related frame is the solar-magnetic (SM) coordinate system. In this system the Z axis is directed to the north

along the geomagnetic dipole axis, and the Y axis is perpendicular to the earth-sun line toward the dusk side. The X axis is not always directed toward the sun in this system, but rocks back and forth through 11.5 degrees about the earth-sun line. This system differs from the GSM essentially by a rotation about the Y_{sm} axis.

In addition to strictly spatial coordinate systems, several so-called magnetic systems have been found useful in studying the motion of charged particles trapped in the magnetic field; these coordinates generally locate particles by reference to surfaces on which some magnetic parameter is constant, and since most particles are strongly controlled magnetically a great simplification of the data often results. Most widely used is the B-L coordinate system of McIlwain. As shown in Figure 4-4, surfaces of constant B (magnetic field intensity) are concentric, roughly ellipsoidal shells encircling the earth, while surfaces of constant L (a magnetic parameter) approximate the concentric shells generated by dipole field lines rotating with the earth. The mathematical definition of L arises from the equations of motion of particles in the field; to some degree of approximation, particles move to conserve three adiabatic invariants to which B and L are simply related. Since these coordinates are more useful to the study of trapped particles than to the study of the field itself, the reader is referred to standard texts on trapped-particle physics for a complete discussion.

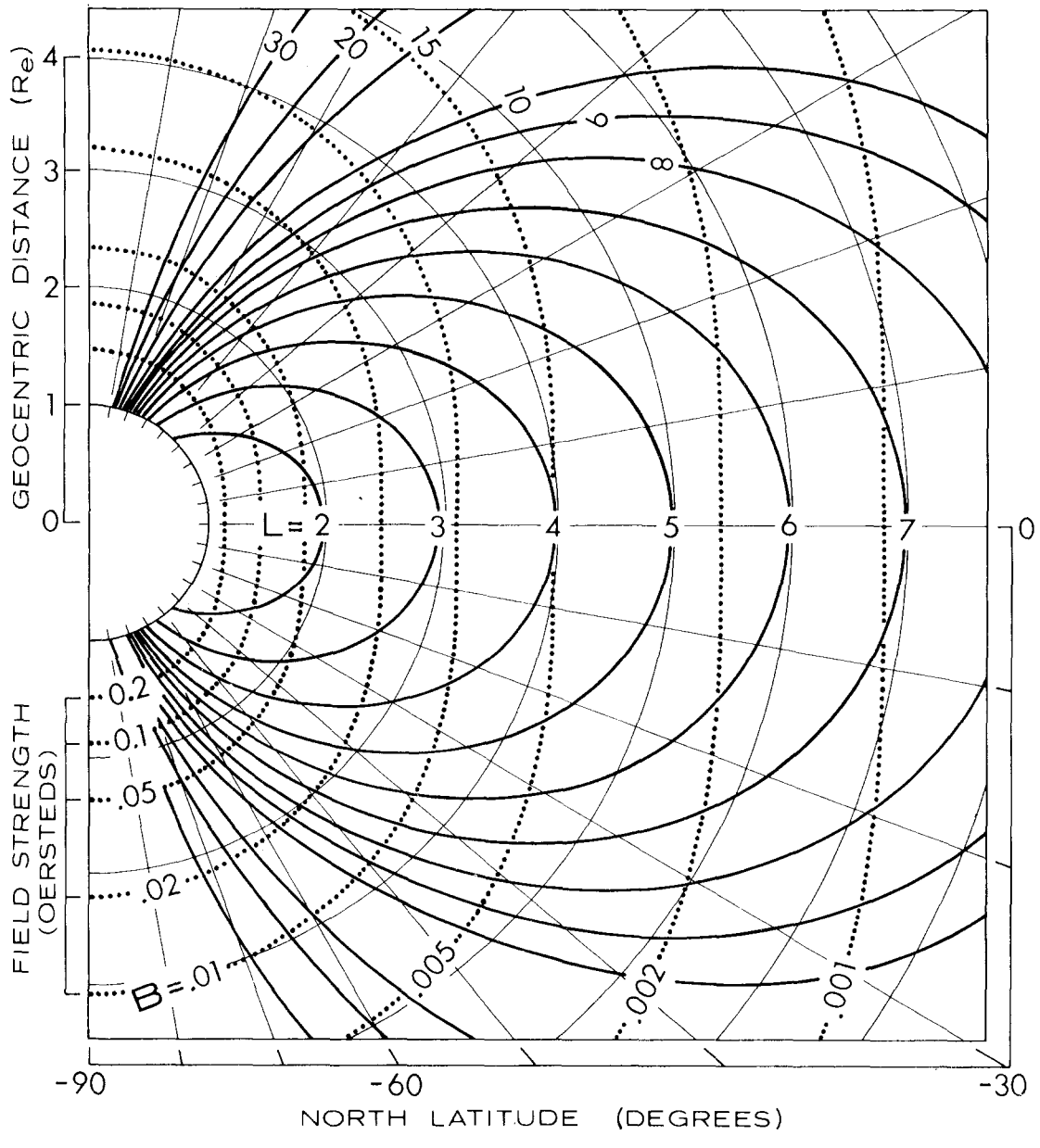

Figure 4-4. The B-L coordinate system. The curves shown here are the intersection of a magnetic meridian plane with surfaces of constant B and constant L. (The difference between the actual field and a dipole field cannot be seen in a figure of this scale.)

4.1.3 Sources of the Geomagnetic Field

In considering a physical description of the field, a useful point of view to adopt is that of energy balance. A static field represents an energy density $B^2/8\pi$, and any change in the field implies a transfer of energy to or from the field. Understanding the field therefore implies identifying the energy sources and the causative physical mechanisms through which this energy generates (or is generated by) the field. Except in the case of permanent residual magnetism, a magnetic field is generated only by the macroscopic motion of electric charge, so the final step in any physical process affecting the field will involve electric currents, though the energy driving the currents may be drawn from various sources. At present, the terrestrial and extraterrestrial sources known to contribute appreciably to the geomagnetic field are the following:

1. Core motion. Convection motion of the conducting fluid core of the earth constitutes a self-exciting dynamo.
2. Crustal magnetization. Residual permanent magnetism exists in the crust of the earth.
3. Solar electromagnetic radiation. Atmospheric winds (produced by solar heating) move charged particles (produced by solar ionizing radiation); this constitutes an ionospheric current which generates a field.
4. Gravitation. The gravitational field of the sun and moon produces a tidal motion of air masses that generates a field in the same way as does the air motion from solar heating.
5. Solar corpuscular radiation and interplanetary field. A number of field contributions arise directly or indirectly from the interaction of the solar wind and its imbedded magnetic field with the main field of the earth. Some important effects are the compression of the main field by external plasma pressure, the intrusion of solar plasma into the main field, the heating of plasma already within the field, and the merging of magnetospheric and interplanetary fields.

There are a number of other obvious possible sources that, in fact, do not contribute appreciably; examples are the mantle of the earth and energetic cosmic rays.

4.1.4 The Steady Interior Field

A geometric-temporal description of the field is constructed from measurements made by observatories, stations, ships, rockets, and satellites, all of which are restricted in geometric coverage (geographic or spatial location) and temporal coverage (time period and frequency response). Observed phenomena tend to be classified accordingly. The traditional classification by frequency is very useful and is retained here.

The steady (nonvarying or dc) component of the field may be considered first. Although it is true that the entire field has been varying drastically over geological time scales, that portion which varies with periodicities greater than about a year is customarily considered to be the steady field, while the remainder is considered the variation field.

Most of the steady field arises from internal terrestrial sources (that is, below the surface of the earth, but excluding currents induced in the earth by external current systems) and is known as the main field. This field results primarily from convective motion of the core and is approximately of dipole configuration, having a strength at the surface of the earth of several times 10^4 nT. The dipole is centered close to the center of the earth, with its axis inclined about 11.5 degrees to the axis of rotation. About 10% of the main field, often termed the residual field, is nondipolar; it consists of both large-scale anomalies (up to thousands of kilometers), believed to be generated by eddy currents in the fluid core, and small-scale irregularities (down to 10 km) arising from residual magnetism in the crust. Changes in the main field (the so-called secular variation) are slow, with time constants of tens to thousands of years.

If the earth were in a perfect vacuum, its dipole field would extend outward without limit, merging smoothly with the fields of the sun and other planets in a simple additive fashion, the field strength declining inversely with the third power of geocentric distance. However, interplanetary space is not a vacuum but is filled with the ionized corona of the sun (the solar wind), which flows continuously outward past the planets. On a quiet day, near the earth, this plasma typically has a density of a few ions/cm^3 and a velocity of about 400 km/s. An important feature of the plasma is its high electrical conductivity. One result of applicable theory is that the magnetic field will be "frozen into" such a plasma; that is, the ions, electrons, and magnetic field will move together as a compressible fluid medium. When such a moving fluid encounters a stationary entity with which it can interact, such as the geomagnetic field, one or the other will be deflected, swept away, or otherwise modified by the collision. The total pressure of the solar wind is the sum of the pressure exerted by the momentum of the particles and the Maxwell pressure $B^2/8\pi$ of the frozen-in field. The geomagnetic field also contains highly conductive plasma, and this medium similarly sustains a pressure equal to the sum of the ambient-plasma and Maxwell pressures. When the pressures of the interplanetary medium and the geomagnetic field are compared, it is clear that at great distances the geomagnetic field will be swept away by the solar wind and that close to the earth the solar wind will be excluded by the field. At intermediate distances there must exist a region of interaction where the pressures are comparable and where rather complicated features can be expected. In the last decade, satellite experiments and theoretical development have discovered and clarified the principal features of this interaction. Some of them are illustrated in Figure 4-5. (The 23° tilt of the rotational axis and the 11.5° tilt of the dipole

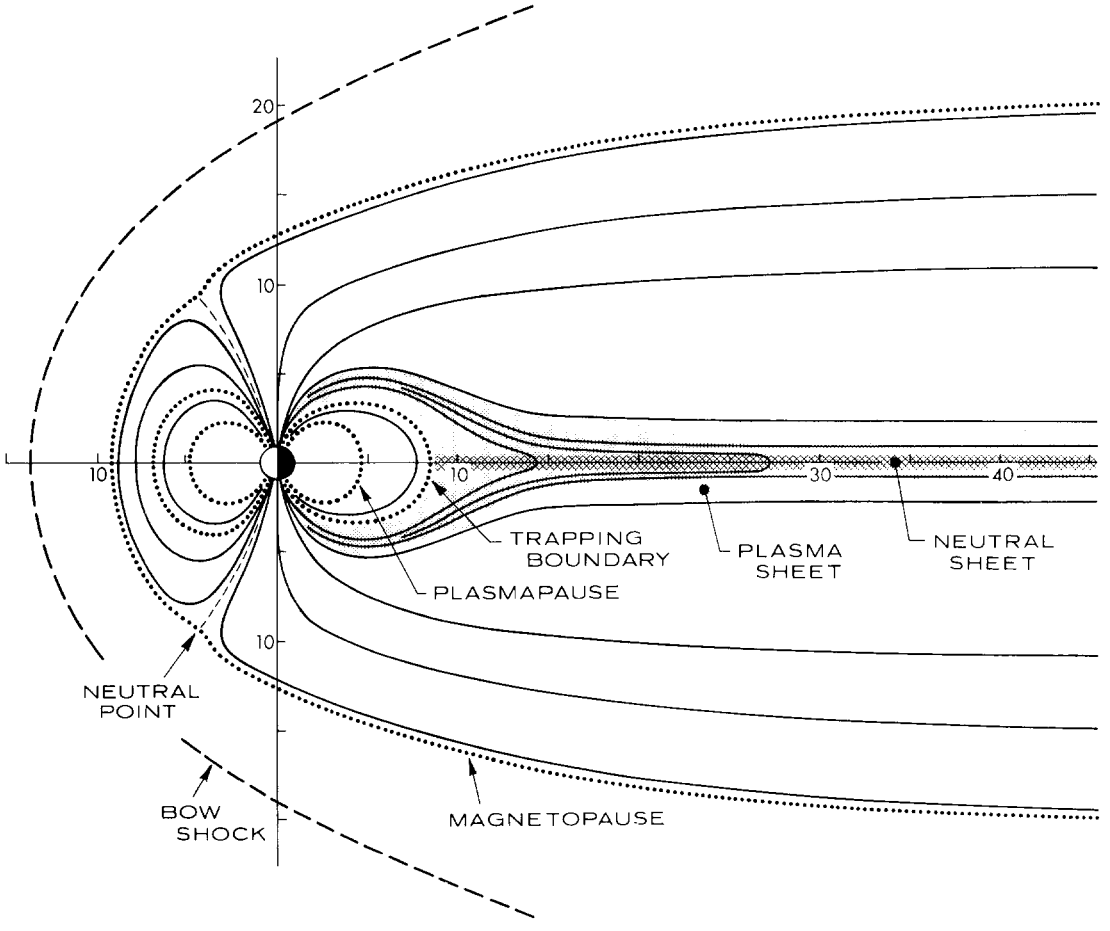

Figure 4-5. The general configuration of the magnetosphere, shown in a noon-meridian section.

axis have been neglected for simplicity.) The field of the earth extends to a geocentric distance of 10 R_E toward the sun (R_E being a unit of length equal to the radius of the earth) at which distance it terminates abruptly in a thin layer known as the magnetopause. The region interior to this layer is known as the magnetosphere. The region exterior to it contains the solar wind, which is "piled up", that is, compressed, deflected, heated, and made turbulent by the collision. These effects propagate some distance upstream, with the result that the wind is slowed over a distance of a few R_E. Since the velocity of the undisturbed wind is "supersonic", there exists a surface at which the velocity is just "sonic" and a stationary shock front, the bow shock, is created. The magnetopause is typically at about 10 R_E and the bow shock at about 14 R_E on the sun-earth line. The region between these is called the magnetosheath. Field lines from the high-latitude (polar cap) regions are swept back toward the night side and form a long geomagnetic tail. Although it might be expected that solar wind pressure perpendicular to the direction of its bulk flow should close the magnetosphere within a few tens of R_E behind the earth, that is not the case; the combined pressure of field and plasma within the tail is sufficient to prevent closing, and the tail has been observed at a distance of more than 1000 R_E behind the earth. It might also be expected that within the tail the north-polar field lines would be smoothly connected across the equatorial plane to the corresponding south-polar field lines, but this also does not happen; these field lines are drawn out into the tail, directed toward the earth above the plane and away from the earth below it. Thus, beyond a geocentric distance of about 10 R_E in the tail, the equatorial plane (neglecting tilts) is a sort of neutral sheet, across which there is a fairly abrupt field reversal, and the component perpendicular to the neutral sheet is very small.

A surface of discontinuity in the magnetic field implies the existence of a current flow in the surface, and the current pattern can be inferred from the field. On the sunward magnetopause the flow is characterized by an eastward current sheet (dawn-to-dusk) across the nose (subsolar point) of the magnetosphere. In the neutral sheet the flow is westward across the tail (also dawn-to-dusk), with return loops on the tailward part of the magnetopause. These currents are shown schematically in Figure 4-6. (The composite magnetopause current is not shown.)

The current system of the magnetopause acts to cancel the dipole field outside and enhance the field inside the

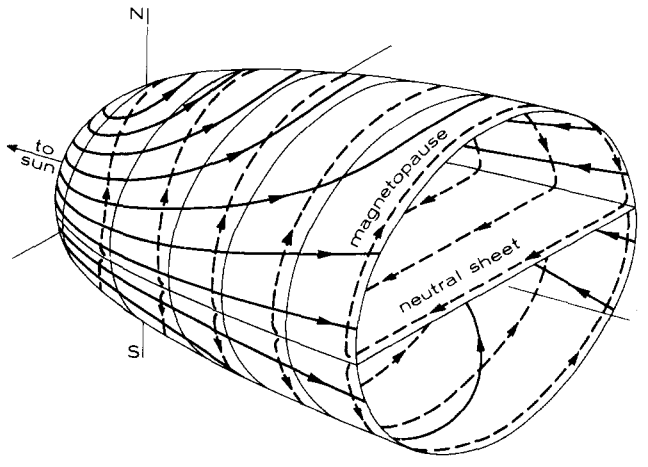

Figure 4-6. Flow patterns of the two principal current systems which determine the configuration of the magnetosphere [adapted after Axford, 1965]

magnetopause. This is equivalent to a compression of the geomagnetic field by the cavity to which it is confined. Because the cavity almost totally surrounds the earth, the field is compressed on all sides, but since the tail is open and the highest pressure is on the nose of the cavity, the compression is somewhat less on the night side. The compression results in an average increase of the equatorial surface field of about 0.1% (about 30 nT); just inside the magnetopause the increase is 100% (which is about 30 nT when the magnetopause is at 10 R_E but about 60 nT if it has been pushed in to 8 R_E). About a third of the surface increase results from diamagnetism in the solid earth.

The steady field then consists basically of the main field of the earth compressed by the cavity to which it is confined. In addition, most of time-varying field contributions discussed below are also (like the magnetopause current) likely to have an average dc value which may be thought of as part of the steady field. For example, convection of the outer magnetosphere and the flowing of a ring current are processes which continue even on the quietest days.

4.1.5 Quiet Variation External Fields

The earth with its core, atmosphere, and main field rotates in the interplanetary environment and moves along its orbit so that any point stationary in geographic coordinates experiences periodic variations in gravity force, solar illumination, and compression or other modification by solar wind effects. The field contributions that result from these motions vary diurnally and seasonally. Field contributions that vary this slowly and regularly and do not result from disturbances in the interplanetary environment are known as quiet variation fields. The analysis of experimental data to determine the quiet variation fields is of course difficult in the presence of magnetospheric disturbance, and criteria for separating field contributions have been somewhat arbitrary and subject to personal judgment. These fields were originally defined on the basis of data taken during a few of the quietest days per month. With better understanding of magnetospheric disturbance, improved measurements, and an awareness that quietness is only relative (any day being only more or less disturbed), it became more common to consider them in an idealized sense as being those variations that would exist if the earth were subjected only to an absolutely quiet external environment. More recently, evidence of a direct connection between quiet and disturbance variations has made this viewpoint less useful.

Quiet variation fields include several contributions. The solar quiet (Sq) variation field, which has a peak-to-peak amplitude of several tens of nanoteslas at most surface locations, is caused mostly by the generation of ionospheric currents by solar electromagnetic radiation. The L (lunar daily) variation field, which typically has an amplitude of a few nanoteslas at the surface, results from the generation of ionospheric currents by luni-solar atmospheric tides. Another contribution of a few nanoteslas at the surface results from the confinement of the main field by the solar wind, the compression being stronger on the day side than on the night side. Quiet variation fields are discussed in Section 4.4, which for both historical and practical reasons retains a ground-based perspective.

4.1.6 Disturbance External Fields

Variations in the geomagnetic field that do not have a simple periodicity and appear to result from changes in the interplanetary environment are called disturbed variation fields or geomagnetic disturbance and are denoted by D. The D field is that remaining after the steady and the quiet variation fields have been subtracted from the total. Large disturbances of relatively long duration, the behavior of which suggests some magnetospheric events as the cause, are termed geomagnetic storms. Except for some fluctuations attributable to irregular motion of the upper atmosphere, the sun is responsible for all disturbance effects recognized at present, and with only two exceptions, it is the solar wind with the frozen-in solar magnetic field that transmits the disturbance to the vicinity of the earth. The two exceptions are disturbances in which ionospheric conductivity is enhanced as the result of solar flares: polar cap absorption events (PCA), which result from low-energy protons from the flare, and solar-flare effects (SFE), which result from x-ray emissions from the flare.

Historically, the disturbance field has been studied by ground observations, with the hope of separating the observed surface field into components that could be explained in terms of current systems above the earth. A useful distinction has been the separation of the component that depends only on universal time (UT) from that which depends

on local time (LT); the former, usually called the storm-time variation and denoted by Dst, is, by definition, symmetric about the polar axis, while the latter, called the disturbance-daily variation and denoted by DS (or Ds), is asymmetric. Then D = Dst + DS. The component Dst was attributed to a ring current encircling the earth a few R_E above the equator, while DS was attributed to ionospheric currents generated by auroral particles precipitated from the ring current. Although better knowledge of the magnetosphere has made clear that ionospheric and magnetospheric current systems are intimately related, this separation is still useful. Other separations have been made or proposed, usually relating to a theoretical model of some postulated physical process. Many are currently in use in the literature but are likely to be revised as understanding improves.

Except as noted above, geomagnetic disturbance results from the interaction of the solar wind with the geomagnetic field. While some minimum level of disturbance may be expected to result from turbulence generated by instabilities in the flow of plasma around the magnetosphere even if solar wind properties were absolutely constant, most disturbance phenomena having characteristic times of minutes to days and observable in ground-based measurements of the field result from variations (often abrupt) in one or more of the solar wind parameters (for example, the density or velocity of the plasma or the direction or intensity of the interplanetary field). The largest disturbances of the magnetosphere are called magnetospheric storms and the corresponding disturbances of the geomagnetic field are called geomagnetic storms. While phenomena vary greatly from storm to storm it is possible to describe a typical or "classic" magnetic storm (see Section 4.5.1). Many other complex dynamic processes in the magnetosphere are manifested in magnetic-field disturbance; some of these are discussed in Chapter 8.

The dynamic behavior of the magnetosphere also includes oscillations, especially in accompaniment to slower magnetic disturbance, both because it is an elastic entity which can resonate and because a number of its dynamic processes generate oscillatory currents. Periodic and aperiodic field fluctuations with frequencies covering nearly eight decades (10^{-3} to 10^5 Hz) are observed. In the lower frequency range (ULF up to 5 Hz) they are called geomagnetic pulsations. These are discussed in Section 4.5.2. Higher frequencies (ELF and VLF) are associated with the dynamics of ionospheric and magnetospheric plasmas.

4.2 MEASUREMENTS OF THE GEOMAGNETIC FIELD

Geomagnetic phenomena are studied experimentally through data obtained by ground stations, ships, aircraft, and space vehicles. This section discusses the instruments used for geomagnetic measurements and reviews the principal sources of such measurements.

4.2.1 Instrumentation

Instruments used over the past several hundred years to measure the intensity and direction of the magnetic field have been few in number and simple in principle, but during the past century they have been made very reliable and fairly precise. Although greater precision and sensitivity were needed earlier, major developments of new instruments came only in the past 35 years, partly because the older instruments were not adaptable for use on rockets and satellites. The principal instruments currently in use may be listed as follows.

Ground-based instruments exploit several physical principles. Several of the older instruments are based on the alignment or oscillation of a permanently magnetized needle in the field; these include the compass, dip circle, and magnetic theodolite, which measure D, I, and H, respectively, the three elements usually measured at observatories to determine the field. Several others rely on the induction of a voltage in a coil of wire. The coil may be rotated in the field as in the dip inductor, or may be fixed as in a large induction-coil magnetometer used to measure geomagnetic pulsations. Two magnetometers are based on the cancellation of a component of the geomagnetic field by the known field of an electromagnet; these are the H-magnetometer of Schuster and Smith and the Z-magnetometer of Dye. Of the newer instruments, several are based on atomic-resonance techniques; these are the proton precession (and proton vector), rubidium-vapor, and helium magnetometers. Another widely used instrument exploits the saturation characteristics of a ferromagnetic core; this is the fluxgate or saturable-core magnetometer. Most recently, a number of extremely sensitive instruments have been developed which utilize the quantum-mechanical behavior of Josephson junctions in a superconducting loop; these are known as SQUID magnetometers (for "superconducting quantum interference devices").

All of these magnetometers are in use for ground measurements. Satellite and rocket measurements rely mainly on the rubidium-vapor, induction-coil (often called searchcoil), and fluxgate magnetometers, which inherently have small size, low weight, modest power requirements, and an easily telemetered output. A brief description of several of the most important of these instruments follows.

Fixed induction coils of various sizes are used to measure rapid fluctuations in the field. To measure the vertical component, horizontal coils with diameters of nearly 10 km are laid out on the ground; for the other components, coils a few meters in diameter, but with many turns, are used. Also used for this purpose are much smaller coils which are wound around laminated mu-metal cores which concentrate magnetic flux for increased sensitivity. Since the quantity measured is the time rate of change of the field, the sensitivity is inherently proportional to the frequency of the fluctuation. A metal-core coil of 30 000 turns, having a diameter of 7 cm and a length of 2 m, can detect variations

of 0.001 nT at one Hz. A typical spacecraft searchcoil having a diameter of 2 cm and a length of 30 cm has a sensitivity 1000 times less.

The first and best developed of the atomic- or nuclear-resonance instruments is the proton precession magnetometer. The physical principle on which it depends follows. Individual protons in a hydrogenous material placed in a magnetic field have both a magnetic moment and an angular momentum, which coincide in direction; the field exerts on the proton a torque tending to align its moment with the field, but the existence of the angular momentum causes the common vector to precess about the field direction. Normally the precessing vectors are random in phase and produce no coherent signal, but if they are started with a common phase by suddenly releasing them after polarization by a strong field perpendicular to the field to be measured, they precess for some time in unison, producing at the precession frequency a signal which can be detected by a pickup coil surrounding the material. The precession (Larmor) frequency is directly proportional to the field, the constant of proportionality being $1/2\pi$ times the proton gyromagnetic ratio. This physical constant, known to an accuracy of better than one part in 10^5, has the value $26751.9 \times 10^5\ T^{-1}\ s^{-1}$ so the frequency for a field of 30 000 nT is 1.2773 kHz. In a typical instrument, the hydrogenous material is a fraction of a liter of water, alcohol, or n-heptane around which is wound a single coil, used first to produce the polarizing field of about 0.01 T and subsequently to detect the precession signal. After the sample is polarized, the coherence of the precession persists for a few seconds before being destroyed by thermal agitation. Several precautions and corrections are required, but the instrument is basically simple and reliable. Absolute measurements of the field can be made with an uncertainty as low as 0.1 nT. The sensitivity of the instrument can be increased to 0.01 nT by adding a microprocessor to process the precession signal. Versions for use in observatories, aircraft, ships, and rockets have been developed and a continuously self-oscillating version is under development.

The proton vector magnetometer combines the proton-precession magnetometer with two sets of Helmholtz coils arranged to null the H and Z components. To measure Z, **H** is first annulled by producing $-\mathbf{H}$ in the H coils. The null cannot be detected directly but is produced by using just half the current required to generate $-2\mathbf{H}$; the latter condition can be detected since the total intensity is then exactly the same as that with zero current in the coil. The current required to annul Z is then measured. First-order instrument errors, of which leveling alignment is most critical, can be corrected by appropriate checks with reversed coils. To keep the field gradient at the sensor low enough with moderate coil dimensions, a four-element Fenselau or Braunbeck coil array may replace the simpler Helmholtz coil. Since this instrument uses the proton precession magnetometer simply as a null detector, the precision of the measurement depends on the accuracy with which the generated fields are known; an uncertainty as low as about 0.3 nT is possible. This instrument is used to measure H and Z at many observatories.

In the last 25 years, a newer resonance instrument has been widely used. This is the alkali-vapor magnetometer, which relies on the Zeeman effect and the phenomenon of optical pumping. Any alkali vapor is suitable, but the rubidium isotopes 85 and 87 have been most used. The energy-level diagram for Rb-87, showing the Zeeman splitting in a magnetic field, is shown in Figure 4-7. When light having a wavelength of about 0.79476 μm is passed through a transparent cell filled with the vapor, resonance absorption and re-emission occurs involving transitions between the various Zeeman sublevels of the ground and first excited states. If the light is circularly polarized, the absorption transitions must have $\Delta m = +1$, so no transitions from the groundstate sublevel with $m = +2$ can occur. Eventually, all electrons are trapped in this substate and no further absorption can take place; the vapor becomes magnetically polarized and transparent. This process is called optical pumping. The polarization can be destroyed by impressing in a direction perpendicular to the ambient field a weak magnetic field oscillating at a frequency (the Larmor frequency) corresponding exactly to the Zeeman splitting (6.99 Hz/nT). Forbidden transitions between the various m-sublevels of the groundstate are induced, electrons trapped in the sublevel with $m = +2$ are redistributed to other sublevels, resonance absorption of the light is again possible, and the vapor is no longer transparent. The ambient magnetic field is determined by measuring the Larmor frequency (that is, the oscillating-field frequency that produces maximum light absorption). The simplest magnetometer consists of the vapor absorption cell surrounded by a coil to produce the Larmor-frequency field, an rf-excited vapor lamp with a filter to absorb all but the 0.79476 μm line, a circular polarizer between the lamp and the cell, and a photodetector to measure the intensity of transmitted light. The frequency of the impressed field may be adjusted manually for minimum transmission of light through the cell; there is a 20% change in absorption between the pumped and unpumped conditions. In more refined instruments, several corrections and improvements are incorporated and they are usually self-oscillating; that is, both the light intensity and the impressed field oscillate with the Larmor frequency, which is established using a feedback signal from the photodetector. The absolute accuracy of alkali-vapor magnetometers is limited by the inherent line width of the resonance (several nT for rubidium) and a further splitting of the Zeeman levels by second-order effects in the coupling of moments; the uncertainty in weak field regions such as the distant magnetosphere is negligible, but in strong-field regions, such as near the surface of the earth, it is seldom less than about 2 nT.

The helium magnetometer also depends on optical pumping. Its operation is similar to that of the alkali-vapor instrument, but since the groundstate of helium has zero

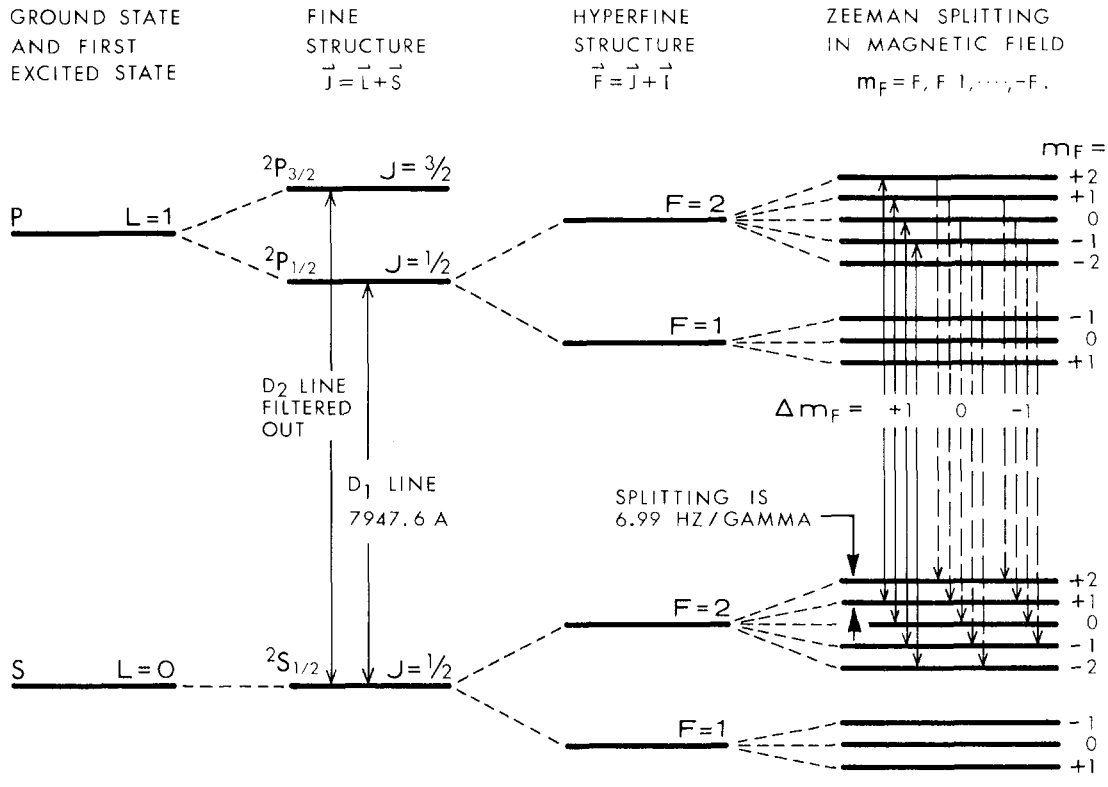

Figure 4-7. Energy-level diagram for Rubidium-87.

magnetic moment, electrons are trapped in a substate of the metastable 2^3P_1 state instead, being excited to the metastable state by an rf electric field. The inherent sensitivity is higher because of a greater Zeeman splitting (28 Hz/nT compared with 7 Hz/nT for Rb-87), but the line width of the resonance is much broader (about 100 nT).

The fluxgate magnetometer has been in use for nearly half a century, but its current usefulness results from extensive development in recent years. At present, it is probably the most widely used instrument in both ground and space measurements for geomagnetic and magnetospheric studies. In its simplest form, it consists of a highly permeable ferromagnetic core on which primary and secondary coils are wound. The primary winding is driven with a sinusoidal current that has an amplitude sufficient to drive the core material into saturation twice each cycle, thus changing the permeability of the material at a frequency twice that of the primary current. The flux in the core has two sources, the exciting field and the ambient external field. The former produces a large component at the driving frequency and, because of the changing permeability, other components at odd-harmonic frequencies. The latter produces a large component at the second-harmonic frequency and smaller components at higher even-harmonic frequencies, all due to the changing permeability; that is, the steady ambient field, which would otherwise produce no signal, is "gated" into the secondary winding by the changing permeability of the core. Since the exciting field produces only odd harmonics, the second harmonic is a measure of the ambient field. Its amplitude is proportional to the magnitude of the field component parallel to the core, and its phase indicates the sign. Several schemes may be used to eliminate the drive signal in the secondary winding. The primary and secondary coils can be wound on axes which are perpendicular, or if the core material is separated longitudinally into two halves, the primary winding can encircle the two halves in opposite senses. In either case the net excitation flux through the secondary can be made zero, and to the degree that this is achieved, only the desired even-harmonic signal is detected. A magnetometer of the latter type is shown schematically in Figure 4-8. Since a single sensor measures only one component, most applications use a three-sensor orthogonal array. It is also common to combine the instrument with coils, either external or wound in the sensor (like the calibration winding shown), to annul all or most of the ambient field. It has also been combined with a servomechanism to orient a three-sensor array such that two sensors read zero, the third measures the total field, and the servomechanism measures the field direction. This so-called orienting fluxgate was used extensively in world-wide magnetic mapping by aircraft. Since the fluxgate is an analog electronic instrument, a number of characteristics of the circuitry and core material limit its absolute accuracy; some instruments have an uncertainty of less than 1 nT. The sensitivity for both ground and space measurements is better than 0.1 nT. Since the excitation frequency may be as high

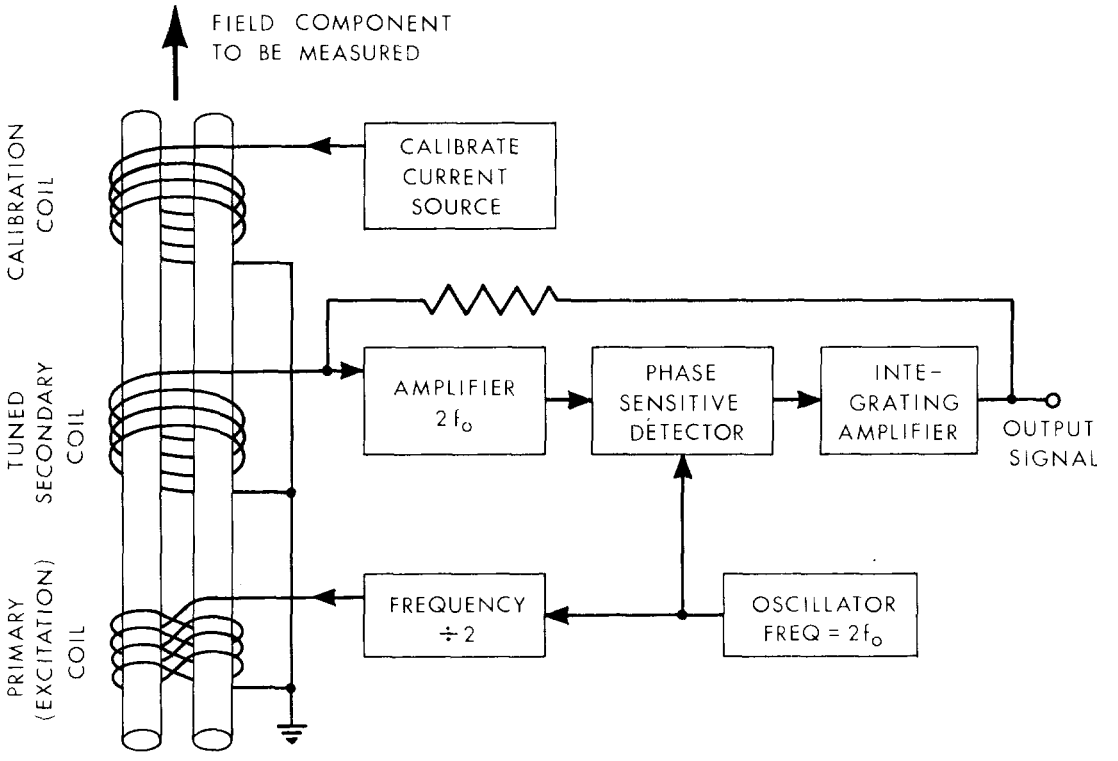

Figure 4-8. Schematic diagram of a typical fluxgate magnetometer.

as 10 kHz, field fluctuations with frequencies as high as 100 Hz or more can be measured.

The most recent and most sensitive instrument is the SQUID magnetometer, which operates in liquid helium at about 4 K. One version uses two Josephson junctions in a superconducting loop as shown in Figure 4-9. Each junction consists of two superconductors (the two halves of the loop) separated by a thin insulator across which a current flows because of the quantum-mechanical tunneling of electrons through the the insulator. Quantum mechanics requires that all electron pairs in the superconductor be in the same state, and therefore that a single wave function describe the entire loop. One result is that in a loop without junctions the magnetic flux enclosed by the loop cannot change (being "trapped") and is quantized in units of $h/2q_e$ (having the value 2.07×10^{-15} Wb), where h is Planck's constant and q_e is the charge of the electron. Adding the junctions to the loop results in a partial breakdown of the trapping; a non-integral multiple of the flux quantum can exist in the loop, but the behavior of the loop in attempting to maintain the trapping can be observed through its effect on the Josephson dc current flowing from A to B in the figure, which varies as shown with the applied magnetic field. Another version requiring only one junction in the loop observes this behavior by its effect on the impedance of a coil arranged to couple an externally generated rf magnetic field into the loop. In either case, the measured quantity exhibits an interference pattern, that is, a series of maxima and minima corresponding to the existence of integral and half-integral multiples of the flux quantum in the loop. The SQUID is not an absolute instrument; changes in the ambient magnetic field are measured by counting the number of maxima which occur in an output signal as the field changes. In practice

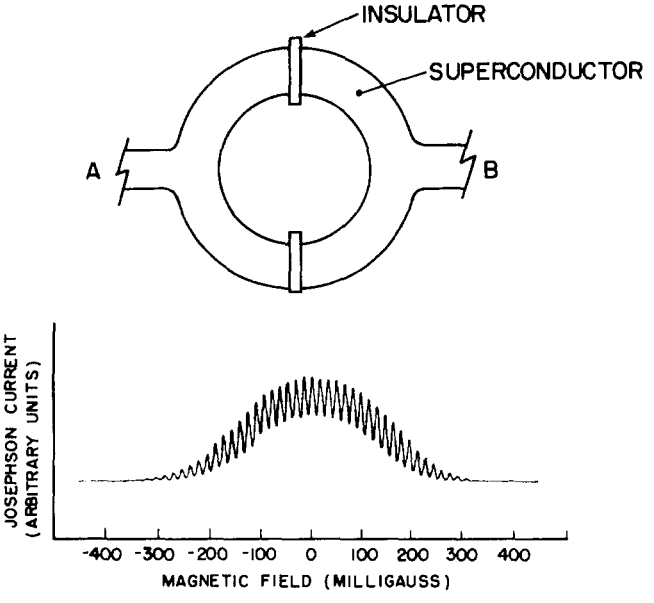

Figure 4-9. The basic geometry and Josephson-current response of a simple dc SQUID magnetometer.

both dc and rf instruments are equipped with feedback circuitry to keep the detector locked on a single maximum, and the amount of the feedback signal becomes the measure of the magnetic field. The SQUID is a vector instrument, since only the component perpendicular to the loop contributes. The sensitivity is extremely high; field changes as small as 10^{-5} nT can be observed. The main limitation is the need to keep the thermal energy kT very small compared with the energy of a flux quantum so the interference pattern is not obscured by thermal noise, and this limits the area of the loop to about 1 or 2 mm^2. The magnetometer inherently possesses excellent linearity, range, and frequency response. Its disadvantages are that it must be calibrated to some other standard, is susceptible to electromagnetic interference (which can cause loss of lock to the reference maximum and hence its calibration), and must be operated in a liquid-helium cryostat.

4.2.2 Ground Measurements

Since the early nineteenth century, the principal source of geomagnetic data has been a continually increasing number of magnetic observatories throughout the world. Recently, the advent of scientific satellites has greatly advanced the precision of global surveys and the study of magnetospheric phenomena, but this has not diminished the need for ground-based measurements.

By 1840 about 50 observatories were making coordinated measurements of the declination by hourly intervals. In recent years over 250 stations have been in continuous or intermittent operation. Of these, over 130 are formal observatories, most of which publish data on a regular basis. Others are repeat stations which are carefully marked and used periodically for standard measurements with portable instruments. Still others are special stations set up for a particular research problem. Their geographic distribution is shown in Figure 4-10, and a list of most stations in recent operation is given in Section 4.8.3. Almost all observatories measure three elements to define the vector field with an accuracy of about 1 nT and a time resolution of one minute. Many also derive K indices and make rapid-run magnetograms for better time resolution. Many of these data are available from the data centers listed in Section 4.8.1.

In recent years, a number of ground-station networks have been constructed to provide the particular geographic coverage needed for the study of ionospheric and magnetospheric dynamics. The largest number were in operation for the three-year International Magnetospheric Study (IMS) commencing in 1977, including five in North America, three in Europe, and (through international cooperation) one which circled the globe. Some are still in continuous or intermittent operation. Data from many of these are in digital form, have 10-second (or better) time resolution, and are available from the National Geophysical Data Center.

4.2.3 Satellite and Rocket Measurements

Sounding rockets carrying magnetometers have been used since 1949 to measure the intensity and height distribution of ionospheric current systems by measuring the change in the transverse magnetic-field component as the current layer was traversed and comparing it with that expected from an idealized infinite current sheet. The equatorial electrojet, the midlatitude Sq currents, and the auroral electrojet have all been studied in this manner using primarily proton-precession or alkali-vapor magnetometers but occasionally fluxgate or searchcoil instruments. Recently, attention has centered on the fine structure of field-aligned currents of the auroral oval, and a series of rocket-borne experiments has attempted to determine the configuration of the lines of force of the geomagnetic field by injecting energetic electron beams along the field line at rocket altitudes and detecting their return.

The use of satellites for magnetic measurements began in 1959 with the Sputnik 3 and Vanguard 3 spacecraft. Measurements since then have provided the drastically altered concept of the magnetosphere described in Section 4.1.4. In the last decade, deep-space satellites with highly elliptical orbits (Hawkeye 1; Heos 1 and 2; IMP H, I, and J; ISEE 1 and 2; OGO 5; and Prognoz 4, 5, 6, and 7) have carried fluxgate magnetometers to the boundary regions of the magnetosphere. Other satellites in elliptical orbits of lower apogee (Explorer 45, GEOS 1, and Jikiken) made measurements largely within the magnetosphere.

Low-altitude polar satellites are ideal for making measurements of the geomagnetic field to derive a spherical-harmonic model of the internal geomagnetic field, since they are nearly simultaneous and have a uniform global distribution. The OGO 6 satellite accomplished this during 1969–1970 using a rubidium-vapor magnetometer to obtain accurate scalar measurements of the field. These were improved on during 1979–1980 by the MAGSAT spacecraft, which obtained both scalar values, using a cesium-vapor magnetometer, and vector component values, using an automatic-field-offset fluxgate magnetometer. The scalar values have an accuracy of 1 nT; instrument and attitude uncertainties limit the accuracy of the vector values to 6 nT.

In the last decade, high-resolution fluxgate magnetometers on the polar-orbiting TRIAD and Air Force S3-2 satellites measured the distribution and intensity of field-aligned currents connecting the outer magnetosphere to the polar and auroral regions of the ionosphere. By applying spin-averaging techniques, data from the fluxgate magnetometers (carried for attitude determination on the ISIS 2, AE-C, and S3-3 satellites) were also used to measure field-aligned currents.

Magnetometers aboard geostationary satellites respond primarily to time variations in the geomagnetic field and have been useful as extraterrestrial observatories to monitor the fluctuations caused by magnetic storms. In the last decade, such spacecraft, all equipped with three-component

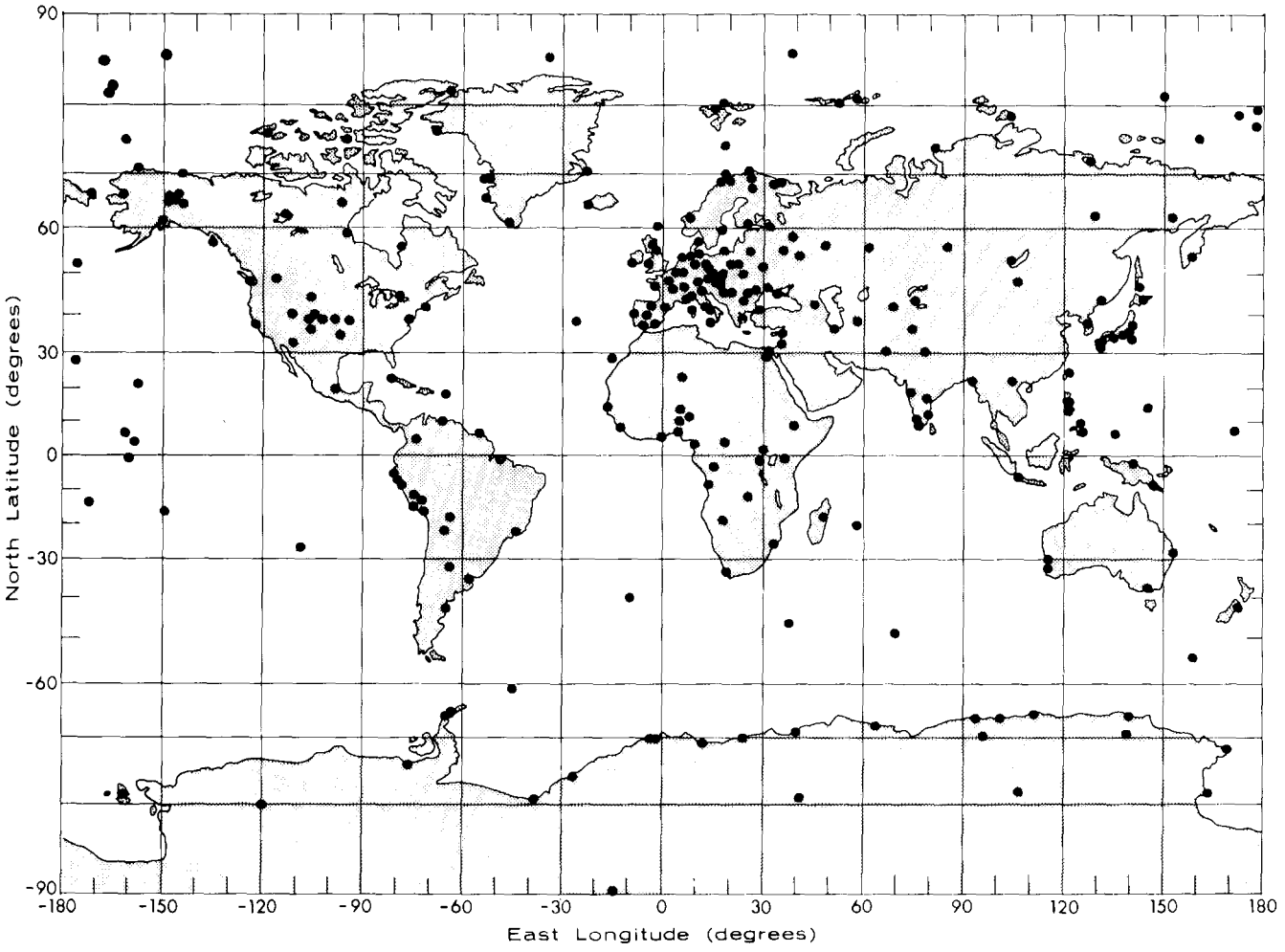

Figure 4-10. Geographical distribution of magnetic observatories.

fluxgate magnetometers, have included ATS 5 and 6; GEOS 2, GOES 1, 2, and 3; SMS 1 and 2; and (in an orbit slightly removed from the synchronous position) SCATHA.

4.3 THE MAIN FIELD

The steady field includes both the main field of terrestrial origin and the nonvarying components of external current systems. While only the former is discussed here, it should be remembered that the latter contributes to the surface field an amount which exceeds the uncertainty of present satellite survey measurements.

4.3.1 Basic Description

The detailed characteristics of the main field are most easily shown in world charts of the elements. Historically such charts were prepared by the hand fitting of curves to observatory and survey data. Now, however, experimental measurements and mathematical models (Section 4.6) are both sufficiently accurate that differences between them are not detectable on world charts of moderate scale, and charts are plotted from the models. Charts of the magnetic elements F, H, Z, and D are presented in Figures 4-11 through 4-14, respectively. These charts for epoch 1980.0 are plotted from the GSFC 9/80 model [Langel, 1982], but differences between all recent models and the actual field are too small to detect on these small-scale plots. Crustal anomalies, which seldom exceed 100 km in extent but are resolved by current models, are similarly unresolved in these plots.

An explanation of the source of the main field must be consistent with seismic and other geophysical data, and many proposed explanations have been discarded on the basis of convincing arguments. The most satisfactory theory is that the field is generated by a self-exciting dynamo system in which an emf generated by the motion of a conductor (molten iron) in a magnetic (excitation) field produces a current so oriented as to produce the excitation field. Although a detailed understanding of core circulations is still lacking, it is believed that the dipole part of the field results

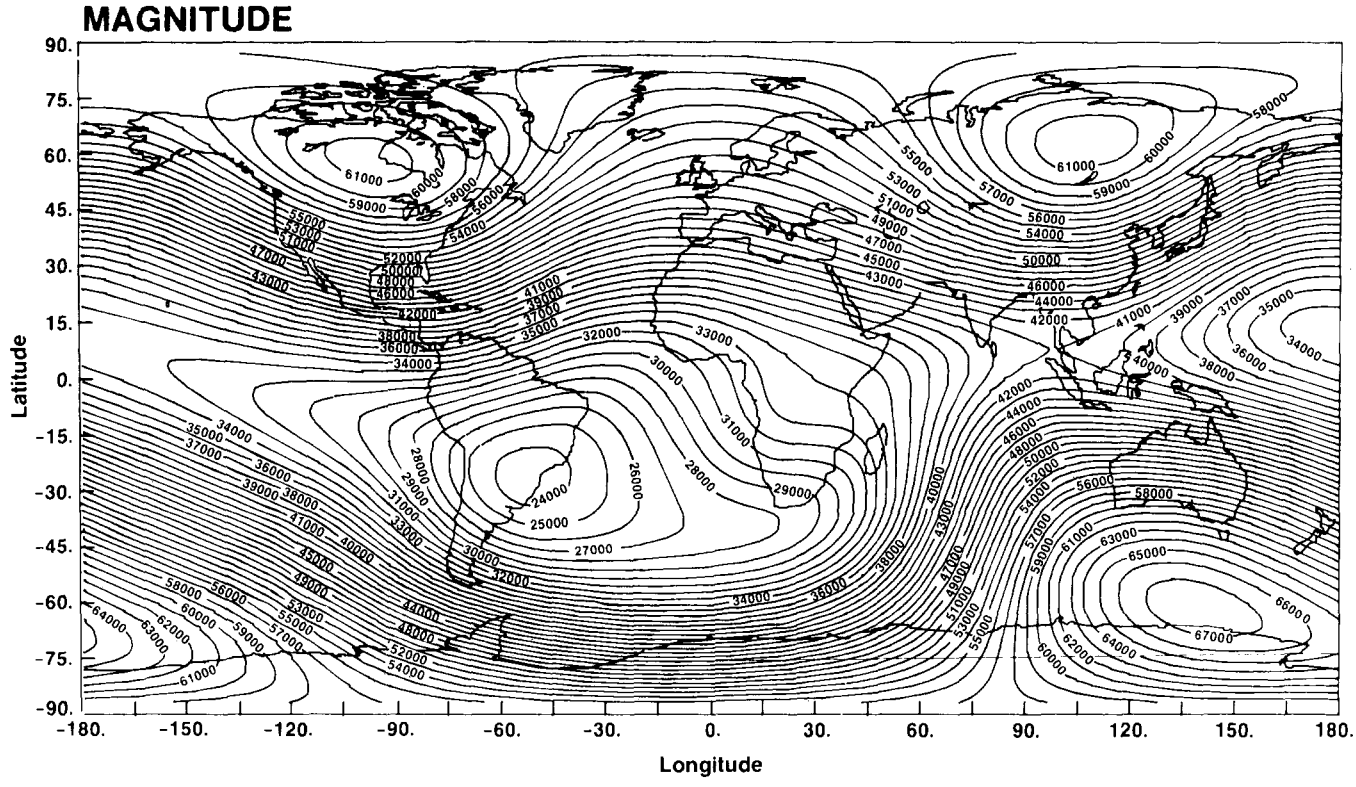

Figure 4-11. Contours of constant total field F at the surface of the earth from the model IGRF 1980.0.

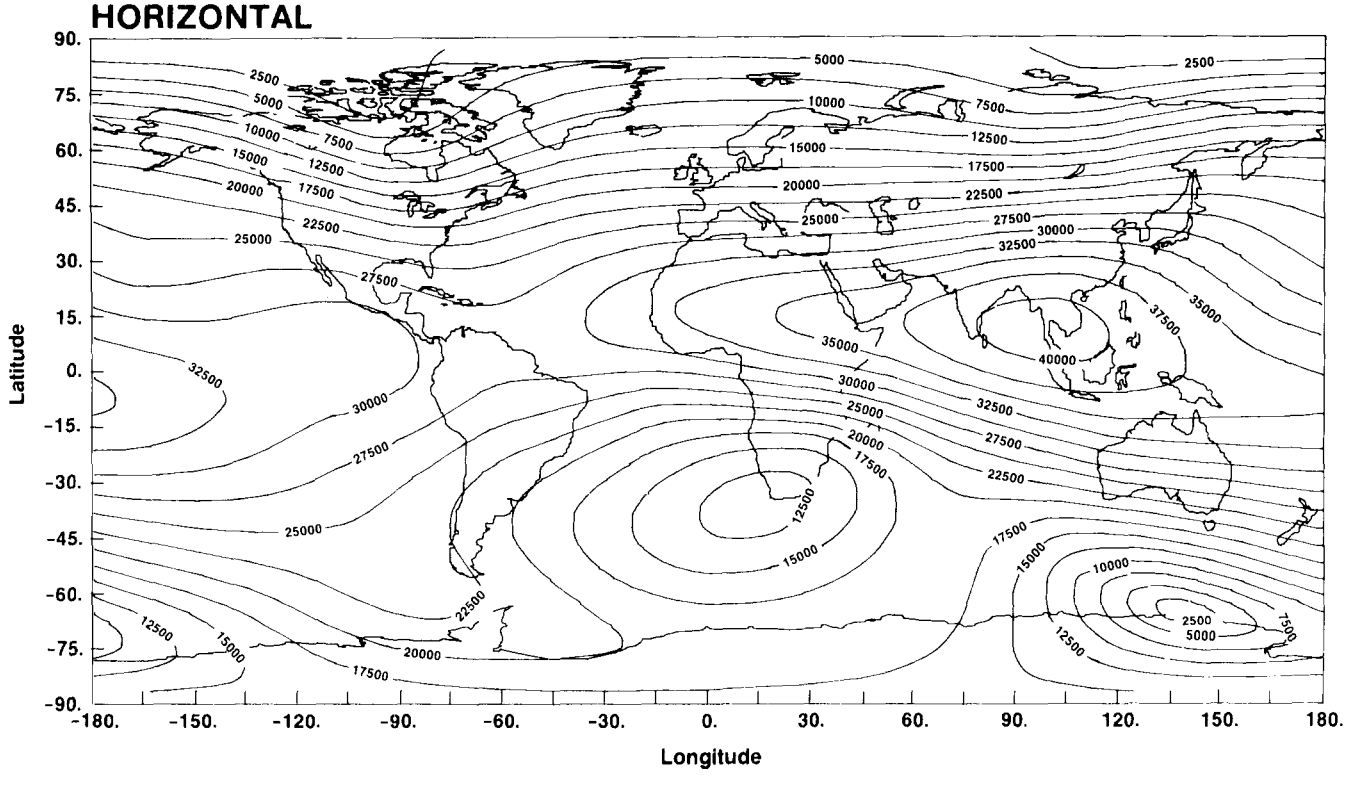

Figure 4-12. Contours of constant horizontal field H at the surface of the earth from the model IGRF 1980.0.

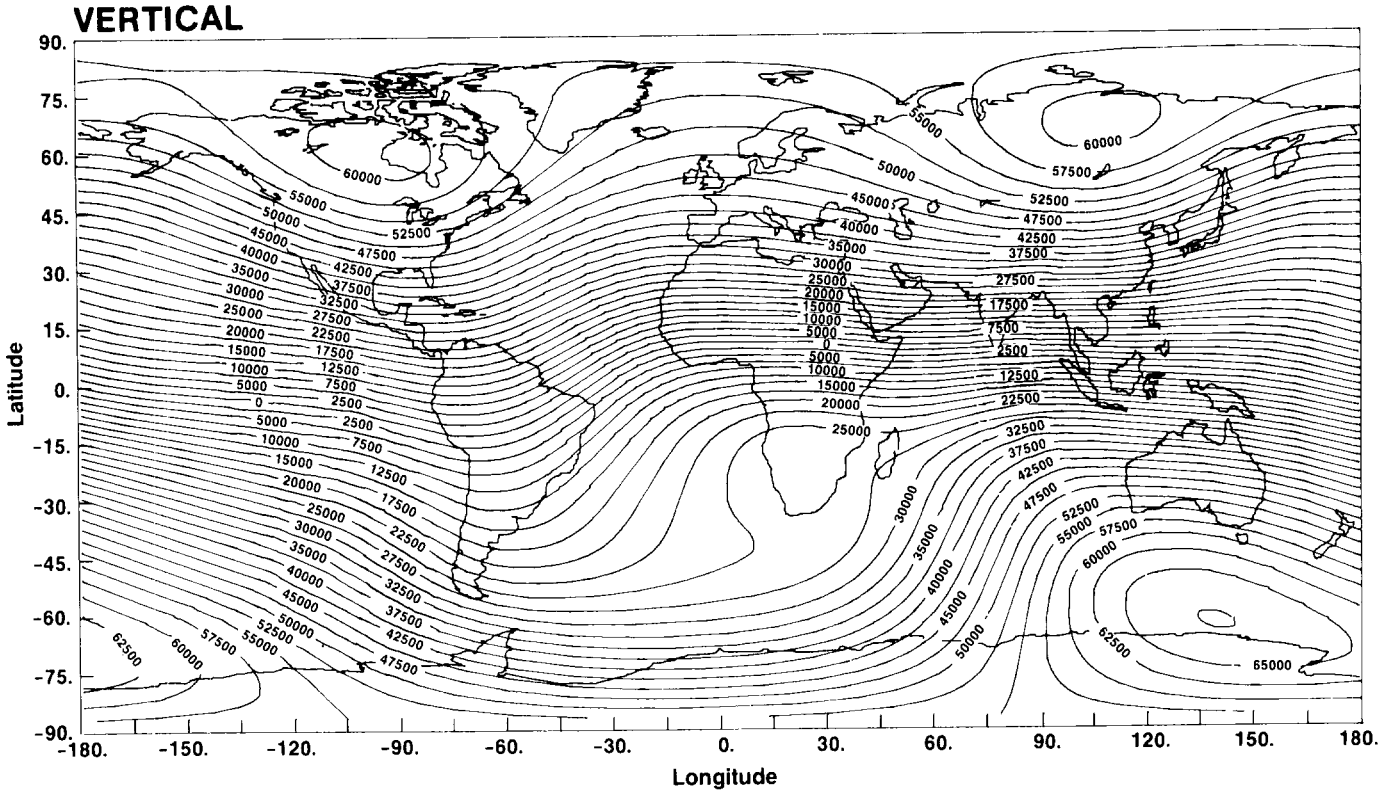

Figure 4-13. Contours of constant vertical field Z at the surface of the earth from the model IGRF 1980.0.

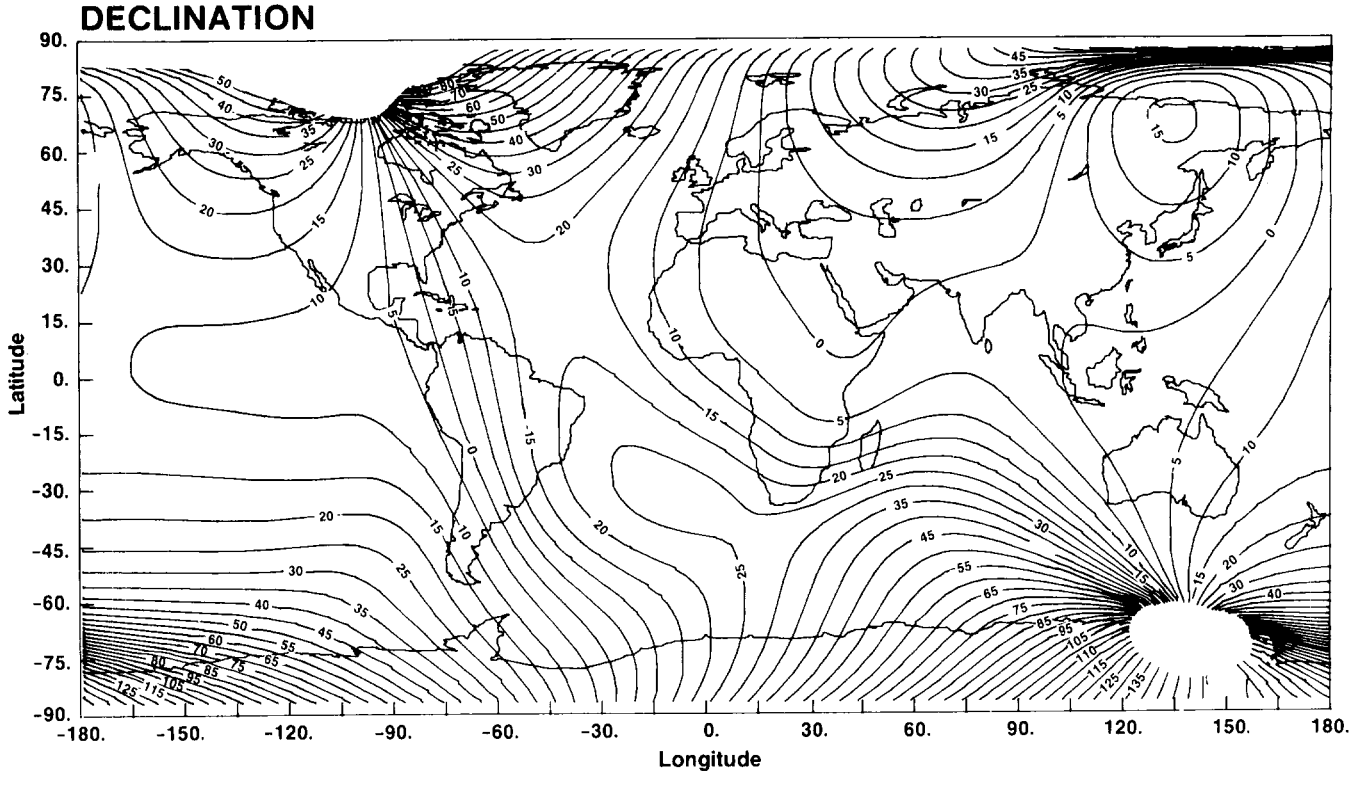

Figure 4-14. Contours of constant declination D at the surface of the earth from the model IGRF 1980.0.

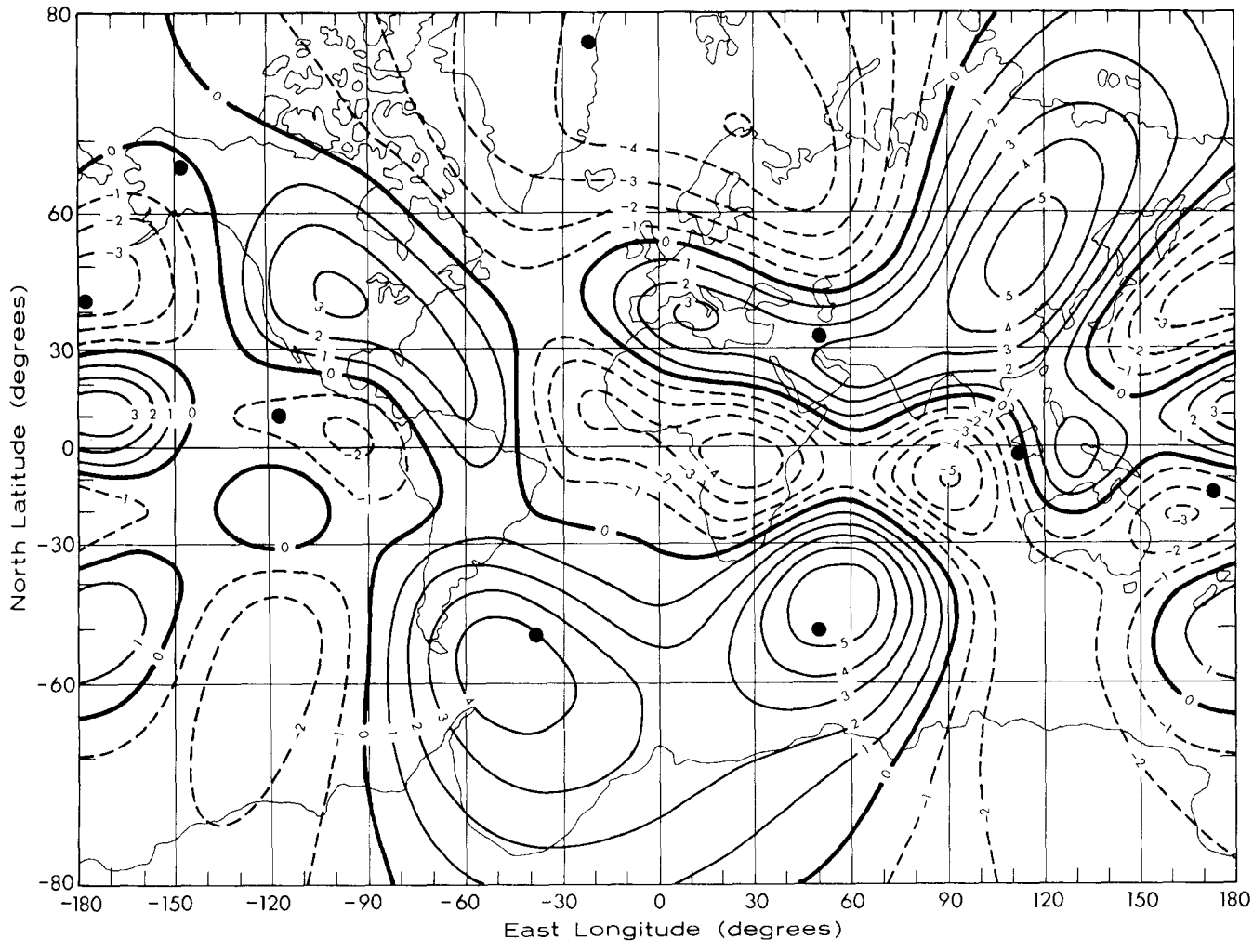

Figure 4-15. The vertical component of the nondipole field, extrapolated to the surface of the core (in oersteds). The locations of nine radial dipoles fitted to the field are indicated by solid circles [see Alldredge and Hurwitz, 1964].

from a major two-dimensional circulation while the nondipole regional anomalies arise from eddy circulations in the outer layer of the core. The regional anomalies can be fitted fairly well by assuming that there exist within the core about nine radial dipoles of various strengths that are equivalent to circulation vortices [Alldredge and Hurwitz, 1964]. These are shown in Figure 4-15. A new analysis of this type will be made of the MAGSAT data [Langel, 1980]. There are also local anomalies of limited extent caused by permanent magnetism in the crust; because this source is so close to the surface, these fields sometimes exceed that arising from the core. The largest is the Kursk anomaly, 400 km south of Moscow, which is shown in Figure 4-16.

4.3.2 The Secular Variation

The secular variation refers to very slow changes in the main field, the time scale generally being measured in years. The variation during the past 400 years or so can be studied on the basis of historical records. For most of this period measurements separated by many years have been required, but current satellite surveys are precise enough to show changes occurring over an interval as short as a year. The variation has traditionally been found by comparing world magnetic charts for successive epochs; it is now derived by computer programs that fit mathematical models to the experimental data from different periods. Defined more narrowly, the secular variation refers to the time derivatives of the magnetic elements of the main field. The secular variation of the total field F is shown in Figure 4-17.

The secular variation observed over recent decades and centuries can be described as the sum of four components that can be described individually: a decrease in dipole strength, a westward drift of regional anomalies, a northward movement of the dipole, and residual nondrifting variations.

Over the entire period of recorded data, the dipole strength

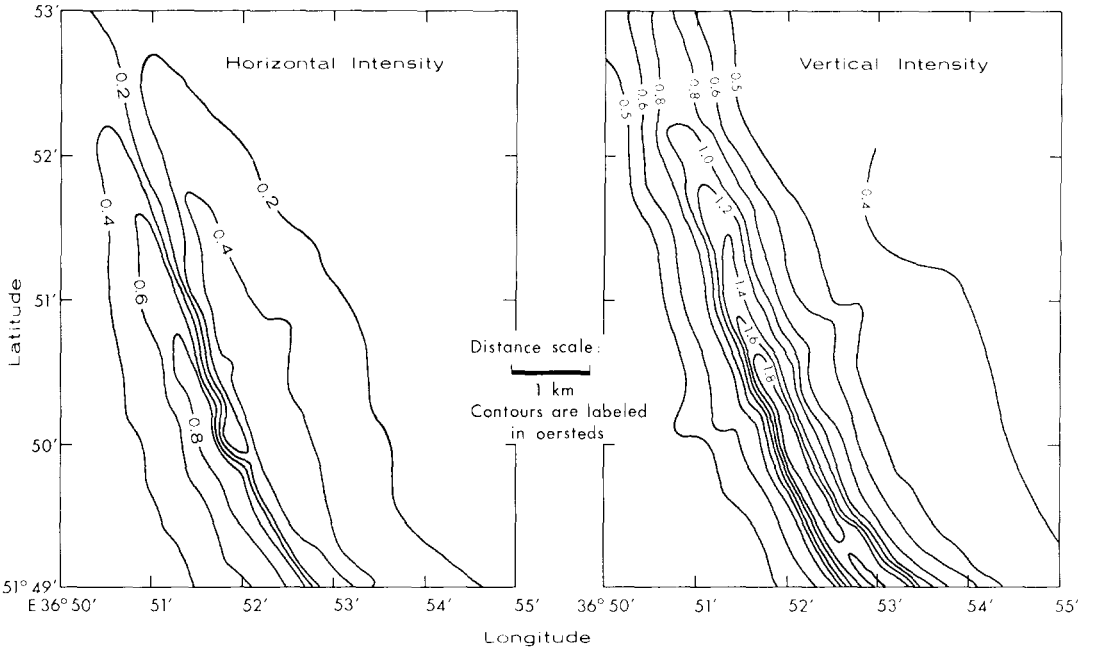

Figure 4-16. The northern portion of the Kursk anomaly. Isointensity contours of the horizontal and vertical field are shown in units of oersteds [after Chapman and Bartels, 1940].

has been decreasing at an average rate of about 0.05% per year (16 nT per year at the equator); data for the past 150 years are plotted in Figure 4-18.

It has long been observed that the major regional anomalies in the field appear to be moving westward, and mathematical analysis [Nagata, 1962] has confirmed that about 60% of the secular variation not attributable to dipole weakening can be accounted for by a westward drift of the nondipole field by about 0.2 degree per year. The cumulative drift over a period of 38 years is easily observed in the equatorial profiles of the vertical field shown in Figure 4-19.

A smaller part of the variation can be described as a northward movement of the dipole center with a velocity somewhat greater than 2 km per year. If this rate were to continue, the center would be outside the core after about 1500 years, so it is likely that the northward motion is merely the current phase of an axial oscillation of the currents that generate the dipole.

The remainder of the variation is relatively small (except in Antarctica). It seems to have about a dozen regional foci, but it has not been accurately measured.

4.3.3 Paleomagnetism

Paleomagnetism, the study of the geomagnetic field in times earlier than those for which recorded data exist, is based on the fact discovered more than a century ago that the natural remanent magnetism (NRM) of some rocks and archaeological samples is a measure of the geomagnetic field that existed at the time of their production. If the NRM is stable, its direction is the same as and its intensity is proportional to the field in which the sample was formed; however, only certain combinations of material, physical process, and conditions result in NRM that is stable enough for reliable results. The most reliable data result from thermoremanent magnetization, locked into the sample by cooling after formation at a higher temperature. The best archaeological samples are baked earths, such as kilns or hearths, from earlier civilizations, and the best geological samples include materials such as lava formed at high temperature. Very careful experimental techniques are required, but the validity of a great many paleomagnetic data and conclusions is well established.

The study of the secular change of geomagnetic-field intensity has been extended backward in time about 5000 years, as shown in Figure 4-20. Over the most recent 2000 years the intensity has tended to decrease at an average rate of about 10 nT per year, while for the preceding 2000 years an increase of similar magnitude is observed.

The study of the secular change of geomagnetic-field direction has been extended backward over both archaeological and geological time scales using data from rock samples. During the past several tens of thousands of years the direction appears to have made quasi-periodic oscillations ranging over several tens of degrees. However, measurements covering the past few millions of years have yielded the important discovery that the dipole axis has not wandered over the entire earth but has remained quite closely aligned

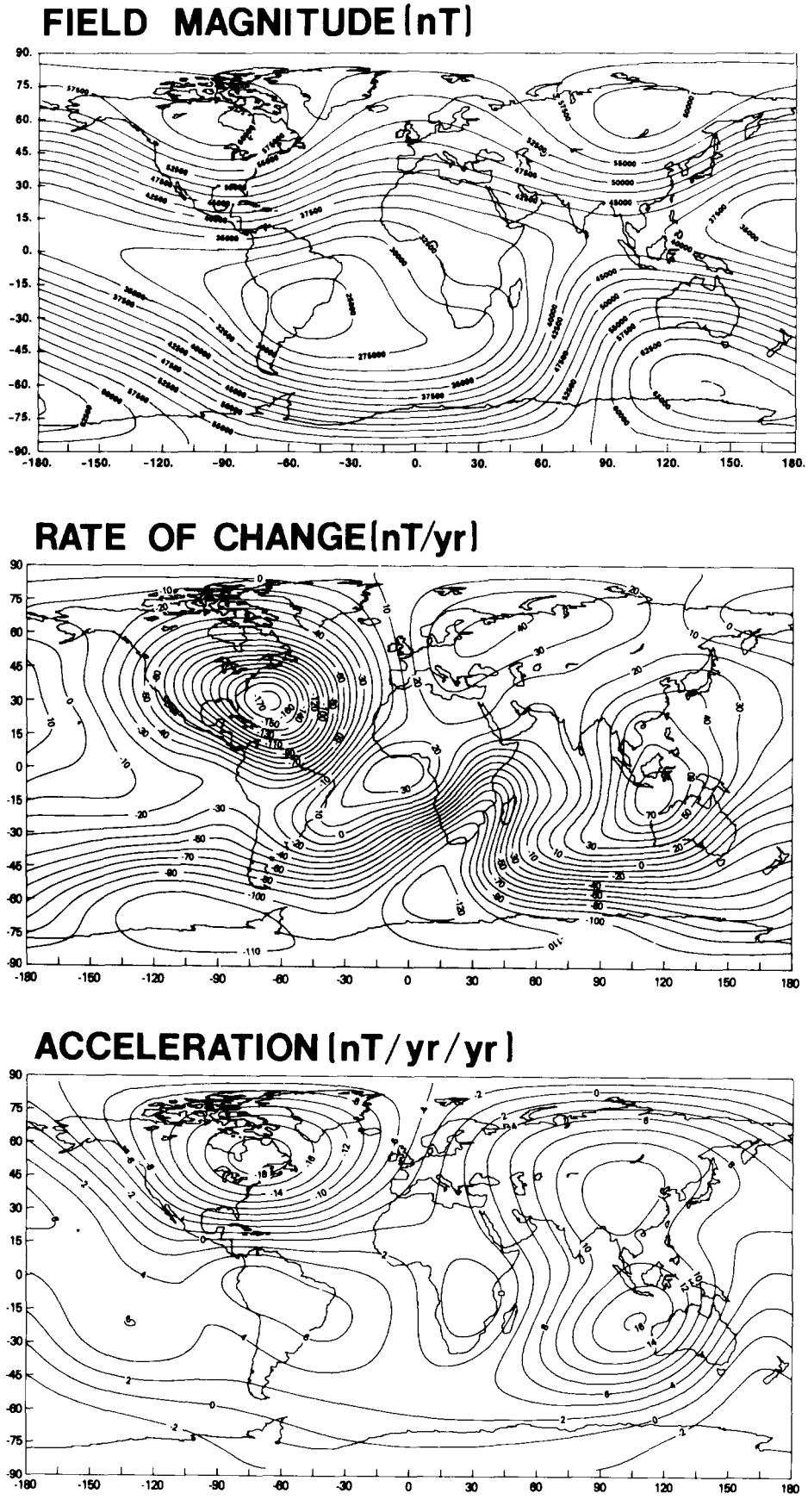

Figure 4-17. The secular variation of the total field for epoch 1980.0. Shown are the field itself (top panel), its first time derivative (center panel), and its second time derivative (bottom panel) [Langel, 1982].

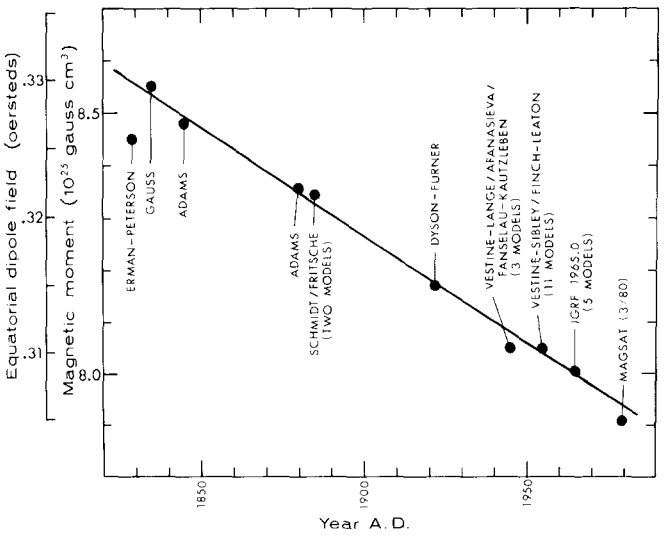

Figure 4-18. Change in equatorial field strength over the past 150 years [historical data from Vestine, 1962].

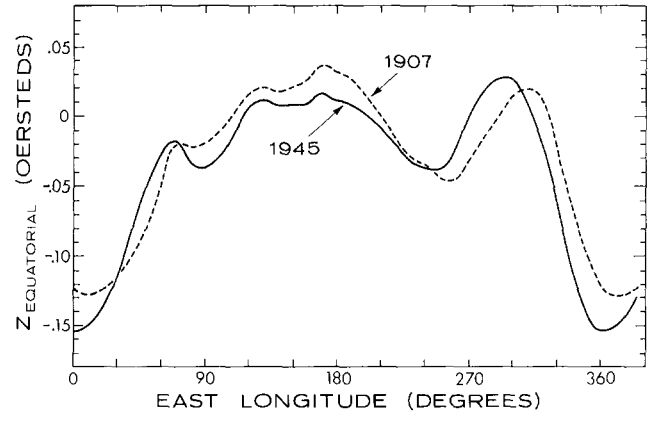

Figure 4-19. Profiles of the vertical equatorial field in the years 1907 and 1945, showing the cumulative westward drift of the non-dipole field over 38 years [after Bullard et al., 1950].

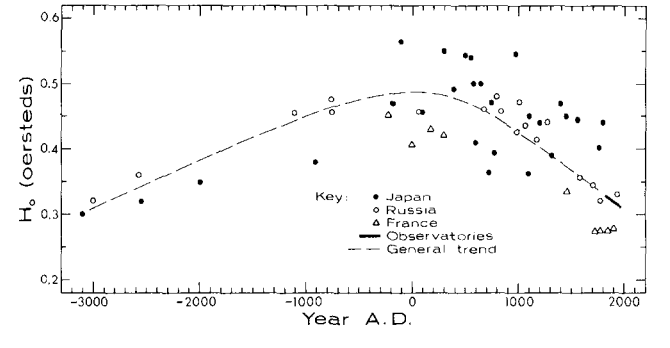

Figure 4-20. Equatorial field intensity in recent millenia, as deduced from measurements on archaeological samples and recent observatory data [after Nagata and Ozima, 1967].

with the axis of rotation. There seems generally to be a clockwise motion of the dipole axis about its mean position with a period of roughly 10 000 years suggesting a precession about the axis of rotation.

For earlier geological ages, paleomagnetic (as well as paleoclimatological) data obtained on any one continent tend to be consistent and yield a time history of the apparent motion of the magnetic poles; over hundreds of millions of years, such "virtual poles" seem to have moved systematically by many tens of degrees toward their present locations. However, there is a very large apparent disagreement between traces for different continents. The explanation is that during this time period the continents themselves have drifted large distances from their original locations.

Measurements covering about 500 million years have revealed that there exist reversely magnetized rocks, and careful study has established that these indicate that the field has periodically undergone complete reversals, the latest being only about one million years ago. It is not clear whether the present weakening of the dipole field represents the beginning of another reversal or a less drastic oscillation.

4.4 QUIET VARIATION FIELDS

A daily variation of the surface magnetic field was first noted in 1722. Although the ionosphere was not discovered until 1902, it was predicted as early as 1882 that the cause of the variation was electric current in a conducting layer of the atmosphere. Subsequent study has shown that the quiet variation includes a large effect of solar origin, a smaller effect of lunar origin, and a still smaller remainder due to other magnetospheric processes.

4.4.1 The Solar Quiet Daily Variation

The solar quiet daily variation (the Sq field) results principally from currents flowing in the E layer of the ionosphere. To a first approximation, this current system is stationary in nonrotating coordinates, and the field variation is observed on the ground as a function of local time because the earth rotates under the currents; therefore, it is similar for all observers at the same latitude, having the dependence shown in Figure 4-21. However, this is a poor approximation since the conductivities that determine the current pattern are controlled by the magnetic field, which is tilted, and the Sq variation is more nearly the same along contours of constant dip latitude than at constant geographic latitude. There is also a longitudinal dependence from such effects as the influence of ocean areas upon the strength of induced currents.

Both the conductivity, which permits this current to flow, and most of the electric field, which powers the current, are produced by solar electromagnetic radiation. The

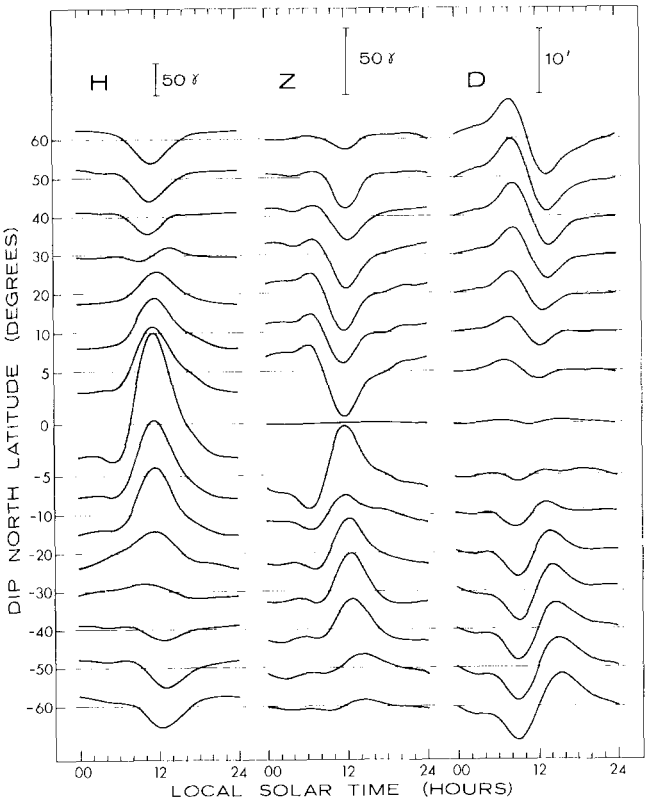

Figure 4-21. Worldwide average of the solar quiet variation near the equinoxes at solar maximum (March, April, September, and October, 1958) [after Matsushita, 1967].

major part of the electric field appears to be generated in the manner of a dynamo by high-speed tidal winds produced by solar heating of the atmosphere, resulting in a variation termed Sq^O. However, it is also clear that part of the electric field, particularly the high-latitude part, originates in the magnetosphere and is communicated to the ionosphere by field-aligned currents resulting in a variation termed Sq^P [Matsushita, 1975]. Figure 4-22 shows the Sq^O and total Sq (Sq^O + Sq^P) ionospheric current systems inferred from a global array of measurements. Induced earth currents (not shown) contribute roughly one-quarter to one-third of the total Sq field.

One notable feature is a concentration of current at the magnetic dip equator. This so-called equatorial electrojet is, in fact, only a few hundred kilometers wide, more concentrated than can be reproduced in the figure by the spherical-harmonic model used to compute the currents. The electrojet exists because of a special circumstance. The fact that the field at the dip equator is exactly horizontal creates a narrow belt of high conductivity in the following way. An electric field impressed perpendicular to a magnetic field (here eastward and northward, respectively) would normally produce a Hall current flowing perpendicular to both (here vertically). However, in this case the conductive medium is bounded in the vertical direction, the Hall current is inhibited, and a polarization results. It is found experimentally and theoretically that the polarization enhances the effective conductivity in the direction of the electric field (Cowling conductivity). At all other points, even slightly off the dip equator, the conductivity along the slightly tilted field lines is sufficient to allow the polarization to leak off partially, and the Cowling conductivity is much less enhanced.

Both the strength and pattern of the Sq variation show a dependence on longitude, season, year, and solar cycle [Matsushita and Maeda, 1965a]. The dependence on season is strong, with the current vortex in a given hemisphere becoming more intense during its local summer. The dependence on solar cycle is also strong; while E-layer ionization increases by 50% from solar minimum to solar maximum, the Sq variation increases by about 100%, presumably because the wind speed also increases. The Sq variation is enhanced and diminished by the changes in solar radiation produced by solar flares and eclipses, respectively.

The Sq field also exhibits large changes from day to day, but the reasons for this are not yet well understood. The current evidence that the Sq current system is partially driven by magnetospheric processes associated with disturbance phenomena blurs the traditional distinction between quiet variation and disturbance variation fields.

4.4.2 The Lunar Daily Variation

The lunar daily variation (the L field) is generated in the same manner as the Sq field, except that the responsible winds are produced by luni-solar gravitational tides and there is currently no evidence for any contribution to the electric field by magnetospheric processes. The dominant behavior is a semidiurnal variation; the amplitude is about an order of magnitude smaller than the Sq amplitude. As in the case of Sq, about 30% of the L field is produced by induced earth currents. Figure 4-23 shows the average L variation in the elements H, Z, and D near the time of an equinox and for a mean lunar age. Figure 4-24 shows the inferred ionospheric (but not induced) currents. A lunar equatorial electrojet is a principal feature, existing (and being more intense than shown) for the same reasons given in the case of the Sq variation.

The dependence of L on several parameters is consistent with expectations [Matsushita and Maeda, 1965b]. There is a seasonal dependence, as for Sq, and also a dependence on lunar age. The solar-cycle dependence on L is smaller than that of Sq, the variation being about 30% (instead of 100%) greater at solar maximum than at solar minimum because the increased activity increases only the conductivities and not the tidal wind speeds. The longitudinal dependence, if it exists, is too small to have been established to date.

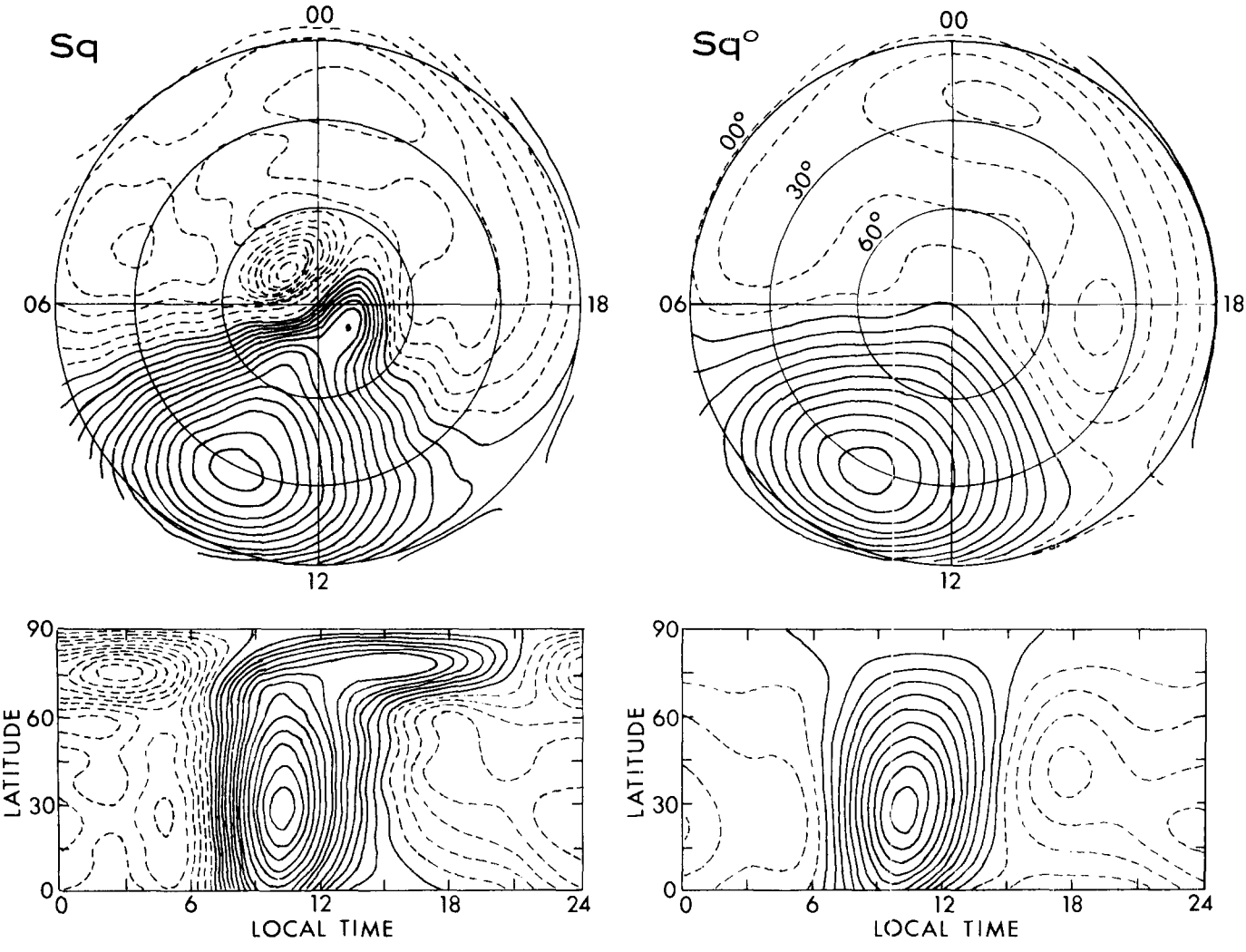

Figure 4-22. Ionospheric currents inferred from the observed Sq variation. The right panels include only the tide-produced currents (Sq^0). The left panels include the convection-produced polar currents ($Sq = Sq^0 + Sq^p$). The current between adjacent solid (broken) contours is 10 000 amperes counterclockwise (clockwise) [Matsushita, 1975].

4.4.3 Magnetospheric Daily Variation

Except for the contribution to the high-latitude Sq field, the daily variation in the surface field that results from the rotation of the earth within its magnetosphere has not been observed directly since it is similar to and certainly smaller than the Sq and L variations. The dayside-nightside difference in compression of the field by a quiet solar wind results in a surface diurnal variation computed to be about 3 nT, and the surface diurnal components of other magnetospheric fields (such as a quiet-time ring current) that could arise from asymmetric geometries are probably negligible. In the outer magnetosphere, of course, such diurnal effects are large, but measurements made there are usually referenced to a coordinate system that does not rotate with the earth; the effect of the rotating earth is then a somewhat different problem.

4.5 DISTURBANCE FIELDS

4.5.1 Geomagnetic Storms and Substorms

The term geomagnetic storm refers to the geomagnetic effects of a magnetospheric storm, which, broadly defined, is any large prolonged disturbance of the magnetosphere by variations in the solar wind. These storms, observed in recordings (magnetograms) of the surface magnetic field, exhibit great variability and complexity, reflecting the complexity of solar phenomena. However, a classic storm, the features of which are frequently observed, can be described as follows. It includes two energizing parts and a subsequent recovery.

The first part consists of a sudden commencement and an initial phase. These result from a change in compression

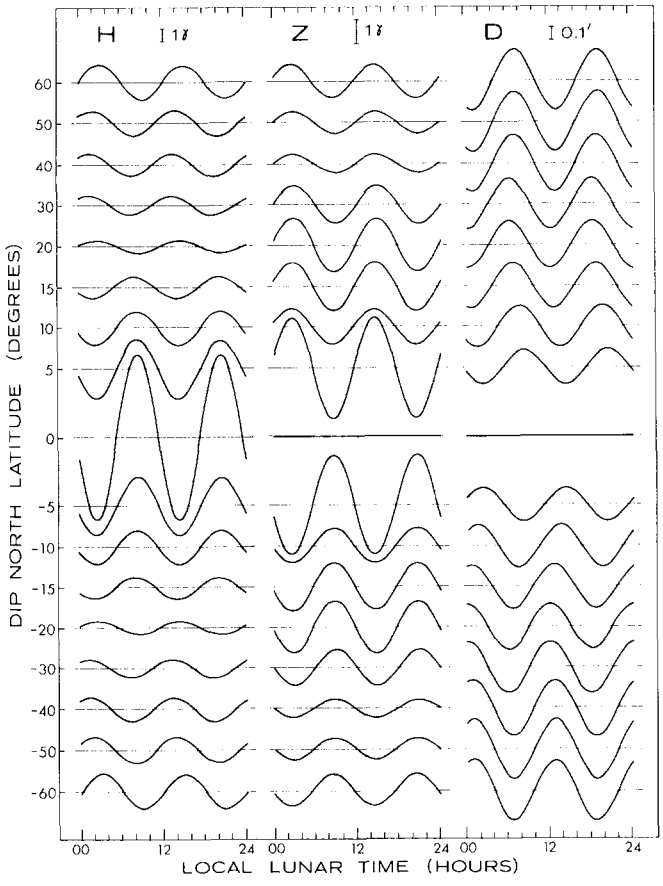

Figure 4-23. Lunar semidiurnal variation near the time of an equinox, derived from data covering the period 1841–1962 [after Matsushita and Maeda, 1965b].

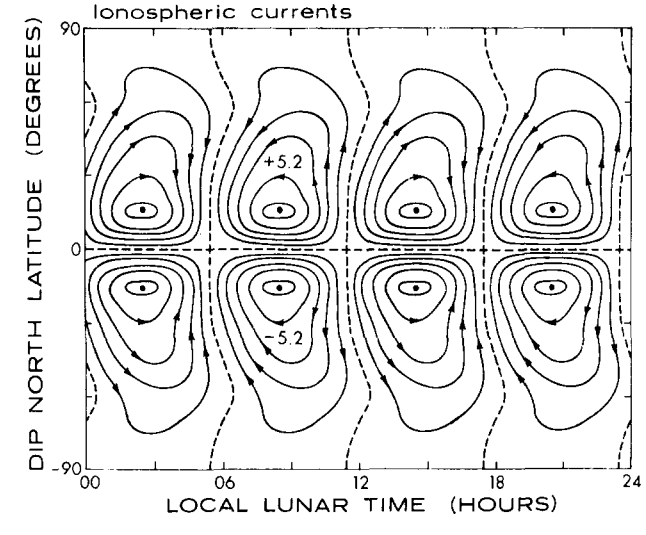

Figure 4-24. Ionospheric currents inferred from the observed L variation. Current between adjacent contours is 1000 amperes, and each dot indicates a vortex center with the total current in thousands of amperes [after Matsushita and Maeda, 1965b].

of the magnetosphere following the passage of a discontinuity such as a shock front propagating in the solar wind and correlate well with the pressure exerted by the bulk flow. The sudden commencement (SC) is seen at low-latitude observatories as an impulsive increase in H, typically having a rise time of one to six minutes and an amplitude of several tens of nanoteslas and observed over the entire earth with a spread in arrival time of less than a minute. Depending on location and the particular storm, it may be positive, negative, double-valued or absent. The rise time corresponds to the time required for the discontinuity to reach all points of the magnetopause and be transmitted to the ground as a hydromagnetic wave. When not followed by the later phases of a storm, this phenomenon is called a sudden impulse (SI). The initial phase typically lasts two to eight hours, during which the field remains compressed by the increased solar-wind pressure following the discontinuity.

The second part is the main phase. It results from an inflation of the magnetosphere by a ring current and is best correlated with a previous southward turning of the interplanetary field, which permits energy to be extracted from the solar wind by a merging of the interplanetary and geomagnetic fields at the magnetopause. It is seen at low latitudes as a rapid decrease in the field to values which are below the prestorm level, often by more than 100 nT and infrequently by more than 1000 nT. It develops over a period of a few hours to a day and is characterized by noise (large fluctuations with a broad risetime spectrum) and an asymmetry in local time (earliest development in the late-afternoon sector). Since solar wind discontinuities usually involve changes in both pressure and field direction, storms typically show both compression and inflation effects, but this is not always the case, and storms without sudden commencements or storms which fail to develop a main phase are not uncommon.

The final part is the recovery phase. It consists of a quiet increase of the field toward the prestorm level with a characteristic time which is typically about one day but sometimes much longer; the recovery is often faster at first than later. Recovery results from a decrease in the ring-current plasma when the source is terminated and the existing plasma is lost by various mechanisms.

The term magnetospheric substorm denotes a process by which energy extracted from the solar wind and stored in the magnetosphere is dissipated. It is so named because the main phase of a large magnetic storm often appears to be the superposition of many substorms, each of which contributes particles to the main-phase ring current. The intermittent and impulsive nature of the substorms accounts for the characteristic noise of the main phase. The substorm is the principal instability of the magnetosphere and very common; it is often observed almost daily and is seldom absent for many days. The process takes place near local

midnight and is manifested in auroral and geomagnetic observations by the auroral breakup and the geomagnetic bay. It is now clear that it involves a short-circuiting through the auroral-zone ionosphere (via field-aligned currents) of the cross-tail neutral-sheet current. This permits closed field lines that had been distended by the cross-tail current to relax earthward into a more dipolar shape, carrying with them particles for the main-phase ring current. Substorms appear to be self-limiting, lasting for less than an hour; larger amounts of energy are often dissipated in a sequence of substorms or one substorm with multiple onsets.

Prior to the most recent decade, many studies of geomagnetic disturbance sought to explain various phenomena by constructing "equivalent" current systems confined to the ionosphere. More recently, there has emerged a much better understanding of the importance and general nature of field-aligned currents in the magnetosphere and the intimate connection between ionosphere and magnetosphere. Chapter 8 discusses some of the magnetospheric-ionospheric processes and current systems, including substorms, that manifest themselves in geomagnetic phenomena and that traditionally have been studied from that perspective.

4.5.2 Geomagnetic Pulsations

Variations of the geomagnetic field having periods from less than one to several hundreds of seconds are observed both on the ground and in the magnetosphere. They are ultra-low-frequency (ULF) waves with frequencies below the ion gyrofrequency that propagate as hydromagnetic waves in the magnetosphere. They have commonly been called micropulsations, geomagnetic pulsations, or simply pulsations. Wave amplitudes range from tenths to several hundred nanoteslas, with the largest amplitudes usually occurring in the longer-period waves at high latitudes. Simultaneous periodic variations in particle precipitation, auroral intensity, electric fields, x ray bursts, and particle flux are often observed. The pulsations have been classified into two principal types: Pc (continuous) pulsations, which often have very sinusoidal waveforms, and Pi (irregular) pulsations. More detailed classification is discussed by Jacobs [1970]; further subdivisions and characteristics of the waves are given in Figure 4-25 [Saito, 1978]. The shortest-period ULF waves are thought to result from cyclotron instabilities with charged particles in the magnetosphere. An overview of these waves can be found in Jacobs [1970] and Nishida [1978]. A description of the large variety of higher-frequency (outside the ULF band) plasma waves in the magnetosphere is beyond the present scope; however, useful summaries have been given by Jacobs [1970] and Shawhan [1979]. Several collections of papers presented for review at meetings have been published [Southwood, 1980; Orr, 1981; IAGA, 1982]. Other useful reviews have been given by Saito [1969], Orr [1973], Lanzerotti and Southwood [1979], Shawhan [1979], Southwood [1979], Hughes [1982], Singer [1982], Southwood and Hughes [1983], and Hughes [1983].

Dungey [1954] suggested that the long-period ULF pulsations observed on the ground were hydromagnetic waves resonating on geomagnetic field lines. In the idealized case, field lines can be considered fixed at both ends in a perfectly conducting ionosphere, and harmonic standing waves can exist on flux tubes. In space and on the ground, magnetic observations of spatial variations in wave frequency and polarization characteristics have supported this picture. An approximate expression for calculating the resonance period is given by the so-called WKB or time-of-flight approximation

$$T = \frac{2}{\eta} \int \frac{ds}{v_A(s)} \propto L^4 \left[\sum_i n_i m_i \right]^{1/2} \qquad (4.1)$$

where the Alfvén speed is given by $v_A = B/(\mu_o n_i m_i)^{1/2}$, the integration is carried out between conjugate ionospheres, η is the harmonic number, ds is an element of length along a field line, n_i and m_i are the number density and mass of species i in the plasma, and L is the McIlwain L-shell parameter. This method is least accurate for the fundamental mode but more accurate calculations of eigenperiods have been carried out using the wave equations for low-frequency hydromagnetic waves in a nonuniform magnetic field (for example, a dipole field). The full hydromagnetic wave equations are coupled and have not been solved in general. However, with certain simplifying assumptions (such as considering magnetic perturbations strictly transverse to the background field) they have been solved for poloidal-mode (radial field displacement) and toroidal-mode (azimuthal field displacement) waves. A particularly useful table for calculating eigenperiods of the uncoupled poloidal and toroidal mode waves is given by Cummings et al. [1969]. Solutions in an arbitrary field geometry have been developed by Singer et al. [1981]. The theoretical development of hydromagnetic waves has been discussed more fully by Southwood and Hughes [1982].

Several mechanisms have been suggested as sources of magnetic pulsations; however, it is usually difficult to link a particular wave observation to a specific source definitively. For waves external to the magnetosphere, sources include the Kelvin-Helmholtz instability (wind-over-water) at the magnetopause boundary, quasi-parallel wave excitation where waves upstream of the bow shock penetrate into the magnetosphere, and sudden impulses due to solar wind discontinuities encountering the magnetopause. For waves internal to the magnetosphere, sources include magnetic substorms, real-space or velocity-space gradients in the magnetospheric plasma distribution, ionospheric conductivity discontinuities, and unsteady large-scale plasma convection. Many dayside Pc pulsations probably originate

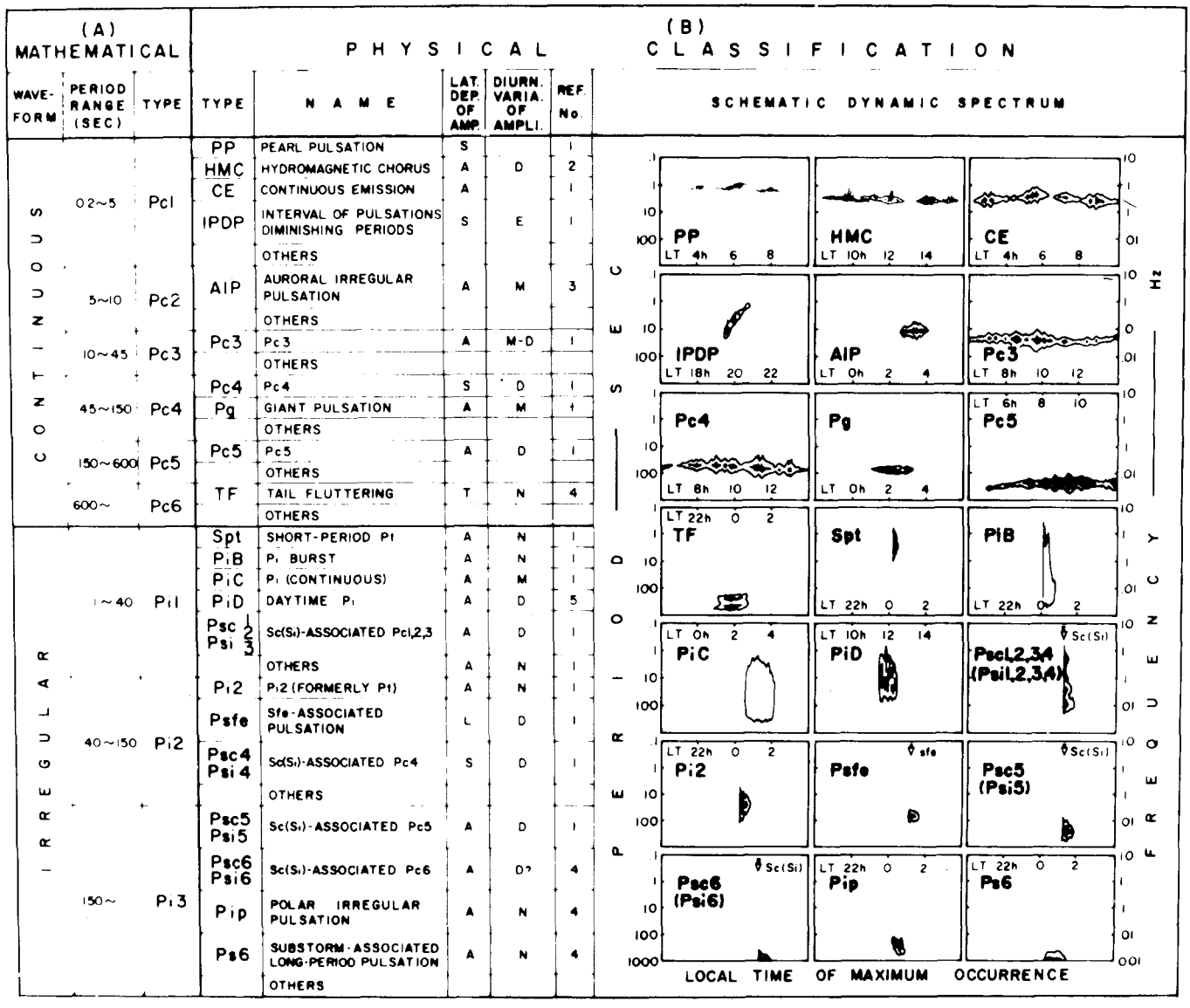

Figure 4-25. Classification of geomagnetic pulsations [Saito, 1978].

as surface waves generated by the Kelvin-Helmholtz instability that evanescently decay inside the magnetosphere where they couple to transverse-mode standing Alfvén waves on resonant field lines [Southwood, 1974; Chen and Hasegawa, 1974]. Pi pulsations are observed primarily on the nightside of the earth and have been clearly linked to the onset of magnetospheric substorms [Southwood and Stuart, 1980].

The ionosphere influences long-period ULF waves in the magnetosphere as well as modifying the signal observed on the ground from that which would be observed in space. Wave energy is lost in the ionosphere through Joule heating by Pedersen currents, and significant amounts of energy may be deposited in the high-latitude ionosphere by waves [Greenwald and Walker, 1980]. The ionospheric Pedersen currents shield the incident magnetic field from the ground, and the signals observed on the ground are due to Hall currents in the ionosphere. A consequence of this is that the polarization of the horizontal wave observed on the ground is rotated by 90° from that which would be observed in space. In addition, the ionosphere acts as a spatial filter and screens short-scale horizontal signal variations $\leq$120 km (approximate height of the E region) from the ground.

The reflection coefficient of an Alfvén wave by the ionosphere is

$$R = \frac{1 - \mu_o v_A \Sigma_p}{1 + \mu_o v_A \Sigma_p} \qquad (4.2)$$

where Σ_p is the height-integrated Pedersen conductivity in the ionosphere, and v_A is the Alfvén velocity along the

oscillating flux tube. The ratio of the effective field-line conductance $(\mu_o v_A)^{-1}$ to the ionospheric conductance is one control on wave damping in addition to wave-particle interactions in the magnetosphere. For example, on the nightside of the earth where $\Sigma_p \sim (\mu_o v_A)^{-1}$, the wave may damp out after only a few cycles, forming Pi2-type pulsations, whereas on the dayside, where $\Sigma_p \gg (\mu_o v_A)^{-1}$, the reflectance is high and waves can exist for many cycles as Pc pulsations. The amplitude of the wave signals on the ground is also controlled by the ionospheric conductivity and the horizontal wave number of the waves. An expression relating the ground field strength b_g to that in the magnetosphere b_m is

$$\frac{b_g}{b_m} \propto e^{-hk\frac{\Sigma_p}{\Sigma_H}} \tag{4.3}$$

where h is the height of the E region, k is the horizontal wave number, and Σ_H and Σ_p are the height-integrated Pedersen and Hall conductivities, respectively.

Magnetic pulsations contain information about their source and the regions through which they propagate. Accordingly, attempts have been made to use ground observations of pulsations as a diagnostic tool for inferring properties of the solar-wind and magnetospheric environments. Ground-pulsation characteristics such as occurrence rate, amplitude, and frequency have been correlated with various combinations of the solar wind velocity and the interplanetary magnetic-field strength and its component values, parameters which are important for generating pulsations in the solar wind or at the magnetopause boundary. Although this reserarch is still in its infancy, it may eventually be possible to monitor solar wind properties from ground-based pulsation measurements, a much easier and less costly technique than *in situ* satellite measurements. Magnetospheric plasma density is another property that would be useful to measure by ground-based observations, and attempts have been made, using the notion of field-line resonance. As can be seen from Equation (4.1), measurement of pulsation period permits determination of plasma mass density along a flux tube, providing the standing-wave harmonic and field geometry are known. This problem is further complicated by the actual distribution of mass on the field line and it does not distinguish plasma species. Nevertheless, it has been used to give estimates of mass density on flux tubes. Another use of pulsations as diagnostics of the magnetospheric environment is that of determining substorm onsets using Pi2 pulsations. It appears that each substorm onset may be associated with a Pi2, although the converse is probably not true. The Pi2 signal is particularly useful because it begins abruptly and can often be observed over a large portion of the earth. In space the signal propagates faster than the plasma injected at substorm onset, and at some distance from the injection source the Pi2 can be used to foretell the arrival of energetic particles.

4.6 QUANTITATIVE MAGNETIC-FIELD MODELS

4.6.1 The Internal Field

A first approximation to the geomagnetic field near the surface of the earth is an earth-centered dipole with its axis tilted to intersect the earth at 78.5°N, 291.0°E, the geomagnetic north pole; the other intersection at 78.5°S, 111.0°E is the geomagnetic south pole. (These values were adopted internationally to define the geomagnetic coordinate system; however, the dipole terms of the first International Geomagnetic Reference Field (epoch 1965.0), also adopted internationally, place the pole at 78.56°N, 290.24°E, and this axis is also sometimes used.) In spherical coordinates, r, θ, and ϕ, with r measured from the center of the earth and θ measured from the dipole axis (geomagnetic colatitude), the dipole field has the vector components

$$\begin{aligned} B_r &= -\frac{M}{r^3} 2\cos\theta \\ B_\theta &= -\frac{M}{r^3}\sin\theta \\ B_\phi &= 0. \end{aligned} \tag{4.4}$$

The total intensity is then

$$B = -\frac{M}{r^3}[3\cos\theta + 1]^{1/2} \tag{4.5}$$

where M is the dipole moment of the earth (about 7.9×10^{15} T/m^3). The equation of a field line is obtained by equating its slope to the slope of the field vector:

$$\frac{r d\theta}{dr} = \frac{B_\theta}{B_r} = \frac{\tan\theta}{2}$$

Integration yields

$$r = r_0 \sin^2\theta \tag{4.6}$$

where the constant of integration r_0 is the geocentric distance at which the field line crosses the geomagnetic equator. A magnetic shell, which is the surface of revolution generated by rotating a field line about the dipole axis, is a useful concept in studying charged-particle motion. In the B-L coordinate system, trapped particles which move adiabatically to conserve three invariants of the motion are confined to a shell of constant L. The B-L coordinate system is, roughly speaking, a transformation of the actual distorted field of the earth into an equivalent dipole field (employing a multipole expansion of the former, as discussed below),

and the shells of constant L transform into the simple magnetic shells of the dipole field, with $L = r_0$.

The centered dipole is a poor approximation to the actual field. It yields an equatorial field intensity of 30 800 nT, while the actual intensity ranges between values of 41 000 and 24 000 nT, more than 25% above and below the calculated value. Much of this discrepancy can be removed by taking the dipole to be eccentric, a fairly good fit being obtained by displacing the center of the dipole 436 km toward 15.6°N, 150.9°E and inclining the dipole axis to intersect the spherical earth at 81.0°N, 275.3°E and 75.0°S, 120.4°E [Parkinson and Cleary, 1958]. However, discrepancies of about 10% remain, which is not good enough for most purposes. Since much better models are readily available for machine computation, the eccentric dipole is seldom used.

Any field derivable from a potential function can be expressed in terms of a multipole expansion of the potential. The coefficients of the various terms can then be adjusted by a least-squares method to give the best fit to the measured field. The methodology for such analyses is well developed, and sets of coefficients along with computer programs to calculate the field and a number of related parameters are readily available. In simplest form, the analysis is as follows. The magnetic scalar potential can be written as a spherical-harmonic expansion:

$$V = a \sum_{n=1}^{\infty} \sum_{m=0}^{n} P_n^m(\cos\theta) \times \left[\left(\frac{a}{r}\right)^{n+1} (g_n^m \cos m\phi + h_n^m \sin m\phi) + \left(\frac{a}{r}\right)^{-n} (A_n^m \cos m\phi + B_n^m \sin m\phi) \right], \quad (4.7)$$

where r, θ, and ϕ are the geographical polar coordinates of radial distance, colatitude, and east longitude, and a is the radius of the earth ($a = R_E$). The functions $P_n^m(\cos\theta)$ are the Schmidt functions:

$$P_n^m(\cos\theta) = \left[\frac{\varepsilon_m (n-m)!}{(n+m)!} \right]^{1/2} \times \left[\frac{(1 - \cos^2\theta)^{m/2}}{2^n n!} \frac{d^{n+m}}{d(\cos\theta)^{n+m}} (\cos^2\theta - 1)^n \right]$$
$$\varepsilon_m = 2 \text{ if } m > 0$$
$$\varepsilon_m = 1 \text{ if } m = 0. \quad (4.8)$$

The second quantity in brackets is the associated Legendre function $P_{n,m}(\cos\theta)$. Its numerical multiplier makes the Schmidt function partially normalized. (Its mean-square value integrated over the sphere is not unity but $(2n + 1)^{-1/2}$). The coefficients g_n^m, h_n^m, A_n^m, and B_n^m appropriate to this function, referred to as "Schmidt coefficients", are now quite universally used in quoting results of analyses, although earlier analyses have used other normalizations, particularly the Gaussian, in which the numerical multiplier is replaced by $[2^n n!(n - m)!/(2n)!]$.

In the potential, those terms containing g_n^m and h_n^m arise from sources internal to the earth, while those containing A_n^m and B_n^m arise from external currents; the potential function is valid in the space above the surface and below the external current system. The field is given by

$$\mathbf{B} = -\nabla V. \quad (4.9)$$

The northward, eastward, and downward components of the field are thus

$$X = \frac{1}{r} \frac{\partial V}{\partial \theta}$$
$$Y = -\frac{1}{r \sin\theta} \frac{\partial V}{\partial \phi} \quad (4.10)$$
$$Z = \frac{\partial V}{\partial r}.$$

The construction of a model consists of adjusting the coefficients g_n^m, h_n^m, A_n^m, and B_n^m to fit experimental measurements taken over a network covering the entire earth, using a least-squares procedure to minimize some quantity such as the weighted sum of the squares of the differences between calculated and measured X, Y, and Z values. As the degree of the multipole terms increases, the magnitude of their effect decreases, and it is pointless to retain more terms than are warranted by the accuracy of the experimental measurements.

Twenty years ago all models were based on surface measurements. Since analyses were unable to identify contributions from external sources, the coefficients A_n^m and B_n^m were usually assumed to be zero. Although measurements were not simultaneous, the existing knowledge of the secular variation was used to adjust them to a common epoch to which the resulting model applied. The significance of coefficients of order greater than about six was dubious.

Since then field models of much greater precision have been developed on the basis of data obtained by low-orbiting polar satellites that can provide nearly simultaneous coverage of the entire earth. A first major advance was made possible by three spacecraft of the NASA POGO series, which carried accurate total-intensity magnetometers. A second advance has now been afforded by the MAGSAT satellite, launched in late 1979, which made accurate three-component measurements of the vector field. The increased precision of these recent data require the retention of higher-

order coefficients in the multipole expansion; the latest models typically include terms to order 13. At satellite altitude (e.g., 500 km), these models specify the field to an accuracy of about 10 nT and clearly resolve regional anomalies resulting from crustal magnetism. Also discernible in the data are the contributions of the external field, including that of the magnetic-storm ring current. Since satellite surveys now span about 15 years, the secular variation can be increasingly well determined. Current models derived from data spanning such a time interval include the time dependence by specifying the coefficients for a reference epoch and also their first and second time derivatives.

Until recently, substantial discrepancies existed between models derived from different data bases. The value of a standard reference field was recognized, and beginning with epoch 1965.0 such a model, the International Geomagnetic Reference Field (IGRF), has been adopted. IGRF 1965.0 was an average model; for any specific purpose another model was likely to provide greater accuracy, but the IGRF served well as a common reference. This difficulty no longer exists; IGRF 1980.0 is the most accurate model available. Its time-derivative coefficients permit its use until 1985 when the next IGRF is scheduled. Retrospective studies have also resulted in a Definitive Geomagnetic Reference Field, consisting of models at five-year intervals (DGRF 1965, DGRF 1970, and DGRF 1975) with linear interpolation of coefficients between them. The DGRF is not expected to be revised further, whereas the IGRF may be (becoming DGRF 1980). A continuous bridge from the DGRF 1975 to the IGRF 1980 is made by the PGRF 1975 ("P" for "provisional"), a linear interpolation between the two. This pattern is expected to be followed for further updates.

The coefficients for the three DGRF models and IGRF 1980 have been published in *EoS* [IAGA, 1981] and elsewhere; those for IGRF 1980 are listed in Table 4-1. These and other field models can be provided by World Data Center A for Rockets and Satellites (Section 4.8.1) in the form of coefficients and computer programs to generate field values.

4.6.2 The External Field

The external field is that portion of the geomagnetic field that results from currents flowing above the surface of the earth. Even at the surface and at low altitudes, where the contribution of the external field is a very small percentage, measurements are now sufficiently precise that it is included in the spherical-harmonic models. As the strength of the internal field weakens with increasing distance from the earth, the external field becomes relatively more important. However, even with external-field coefficients, the spherical-harmonic models described above lose their usefulness beyond about two or three earth radii. The reason is that the geometry of the external field does not lend itself to spherical-harmonic analysis. Therefore, a separate model of the external field must be constructed, and contributions from the internal and external models can then be added to specify the total field at any location in the magnetosphere.

Large-scale current systems, often only partially understood, are associated with many complex magnetospheric processes. However, three major current systems appear to explain the basic configuration of the magnetosphere: (1) the magnetopause current, which creates the magnetopause and flows in it, confining the geomagnetic field to the magnetosphere; (2) the neutral-sheet current, which is driven by the dynamo-generated potential across the magnetosphere and causes polar-cap field lines to be drawn out away from the earth into the tail; and (3) the ring current, which consists of plasma drifting around the earth in the region where field lines have a more dipolar shape. Several useful models have been developed by Olson and Pfitzer [1974, 1977], Tsyganenko [1976], and others to compute the magnetic field produced by these currents. One of the Olson-Pfitzer models includes the tilt of the earth dipole; the other permits varying the strengths of the three currents independently.

External-field models describe a field configuration that is much less stable than the internal field. In studying some magnetospheric process, the model can be used to describe the general field configuration while the process is modeled separately. However, the currents involved in the process may be intimately associated with the model currents. An example is the substorm, in which part of the neutral-sheet current is diverted along field lines and through the ionosphere causing an abrupt change in the configuration of the magnetospheric magnetic field. The development of self-consistent models for such processes is just beginning.

4.7 GEOMAGNETIC ACTIVITY INDICES

The magnetograms and averaged data supplied by magnetic observatories are too detailed for many purposes, and it has long been found useful to compute some numerical parameters that indicate the level of general magnetic activity or of specific types of disturbance. The International Association of Geomagnetism and Aeronomy (IAGA) has formally adopted 19 of more than 30 such indices currently in use. A brief description is given here of several of the most useful indices; a complete review has been given by Mayaud [1980]. The availability and sources of indices are discussed in Section 4.8.5.

4.7.1 General Activity Indices K, Ks, Kp, and Km

The K index, a measure of the irregular variations of standard magnetograms, is an indicator of the general level of disturbance at a given observatory. The index is defined

CHAPTER 4

Table 4-1. Spherical-harmonic coefficients of the IGRF 1980.0.

n	m	g	h	dg/dt	dh/dt	n	m	g	h	dg/dt	dh/dt
1	0	−29988		22.4		8	0	20		0.8	
1	1	−1957	5606	11.3	−15.9	8	1	7	7	−0.2	−0.1
						8	2	1	−18	−0.3	−0.7
2	0	−1997		−18.3		8	3	−11	4	0.3	0.0
2	1	3028	−2129	3.2	−12.7	8	4	−7	−22	−0.8	−0.8
2	2	1662	−199	7.0	−25.2	8	5	4	9	−0.2	0.2
						8	6	3	16	0.7	0.2
3	0	1279		0.0		8	7	7	−13	−0.3	−1.1
3	1	−2181	−335	−6.5	0.2	8	8	−1	−15	1.2	0.8
3	2	1251	271	−0.7	2.7						
3	3	833	−252	1.0	−7.9	9	0	6			
						9	1	11	−21		
4	0	938		−1.4		9	2	2	16		
4	1	783	212	−1.4	4.6	9	3	−12	9		
4	2	398	−257	−8.2	1.6	9	4	9	−5		
4	3	−419	53	−1.8	2.9	9	5	−3	−7		
4	4	199	−298	−5.0	0.4	9	6	−1	9		
						9	7	7	10		
5	0	−219		1.5		9	8	1	−6		
5	1	357	46	0.4	1.8	9	9	−5	2		
5	2	261	149	−0.8	−0.4						
5	3	−74	−150	−3.3	0.0	10	0	−3			
5	4	−162	−78	0.2	1.3	10	1	−4	1		
5	5	−48	92	1.4	2.1	10	2	2	1		
						10	3	−5	2		
6	0	49		0.4		10	4	−2	5		
6	1	65	−15	0.0	−0.5	10	5	5	−4		
6	2	42	93	3.4	−1.4	10	6	3	−1		
6	3	−192	71	0.8	0.0	10	7	1	−2		
6	4	4	−43	0.8	−1.6	10	8	2	4		
6	5	14	−2	0.3	0.5	10	9	3	−1		
6	6	−108	17	−0.1	0.0	10	10	0	−6		
7	0	70		−1.0							
7	1	−59	−83	−0.8	−0.4						
7	2	2	−28	0.4	0.4						
7	3	20	−5	0.5	0.2						
7	4	−13	16	1.6	1.4						
7	5	1	18	0.1	−0.5						
7	6	11	−23	0.1	−0.1						
7	7	−2	−10	0.0	1.1						

for each 3-hour interval on the basis of the largest value R of the 3-hour ranges in X, Y, D, or H, where the range is the difference between the highest and lowest deviations from the regular daily variation. The K value for a given value of R is found from a table in which the location of the station has been taken into account to permit comparison between K values from different stations; the index reflects mainly auroral-zone activity, so stations nearer the auroral zone are much more sensitive. A two-letter subscript identifies the station. The K_{FR} index, from Fredericksburg, Virginia, has sometimes been used as a standard measure of activity for the United States. K values are integers ranging from 0 through 9; the calibration for six representative stations is given in Table 4-2; it may be noted that the K scale is roughly logarithmic with range.

The Kp index ("p" for "planetary") is probably the most widely used of all the indices. It was intended as a measure of the worldwide average level of activity; however, it is very sensitive to certain auroral-zone activity and insensitive to some other types of disturbance. It is based on the K

Table 4-2. Definition of the K scale for six representative observatories

Name of Observatory	Geomagnetic Lat.	Geomagnetic Long.	Lower Limit of R in nT for the K Value to be 0	1	2	3	4	5	6	7	8	9
Godhavn	79.9	32.5	0	15	30	60	120	210	360	600	1000	1500
Sitka	60.0	275.3	0	10	20	40	80	140	240	400	660	1000
Huancayo	−0.6	353.8	0	6	12	24	48	85	145	240	400	600
Fredericksburg	49.6	349.8	0	5	10	20	40	70	120	200	330	500
Tucson	40.4	312.2	0	4	8	16	30	50	85	140	230	350
Honolulu	21.1	266.5	0	3	6	12	24	40	70	120	200	300

Table 4-3. Value of the ap index for a given value of Kp.

If Kp =	0o	0+	1−	1o	1+	2−	2o	2+	3−	3o	3+	4−	4o	4+
then ap =	0	2	3	4	5	6	7	9	12	15	18	22	27	32
If Kp =	5−	5o	5+	6−	6o	6+	7−	7o	7+	8−	8o	8+	9−	9o
then ap =	39	49	56	67	80	94	111	132	154	179	207	236	300	400

indices from 12 stations between geomagnetic latitudes 48° and 63°, selected for good longitude coverage. Values of K are first used to find the Ks index ("s" for "standardized") from tables which remove the characteristic seasonal behavior at the station. The Ks index ranges continuously from 0.0 to 9.0 but is quoted in thirds of an integer by use of the symbols −, o, and +, such that the interval, for example, from 3.5 to 4.5 includes the Ks values 4−, 4o, and 4+. Ks can therefore assume the 28 values 0o, 0+, 1−, 1o, 1+, . . ., 9−, 9o. The Kp value for each 3-hour interval is the average of Ks from the 12 stations. The Kp index is published in two forms: numerical tables and the "musical-note" diagram reproduced in Figure 4-26; in the diagram each successive solar rotation is plotted under the previous one to expose 27-day recurrences of activity.

A newer index Km ("m" for "mondial", meaning global) has recently been developed as an improvement on Kp. It is an average of two component indices Kn and Ks (not to be confused with the standardized K index Ks) derived from northern- and southern-hemisphere stations, respectively. Some of its advantage lies in a simpler and more direct conversion of the data, but the major improvement comes from a much better geographical distribution of stations.

4.7.2 Related Indices ap, Ap, ak, Ak, am, and aa

Because the 3-hour K-type indices are defined with a roughly logarithmic scale, they are not suitable for simple averaging to obtain a daily index (though this is not uncommonly done). To convert to a roughly linear scale (that is, reconversion to an equivalent range), the ap index is defined from Kp by use of Table 4-3, and the daily index Ap is then defined to be the average of the eight 3-hour ap indices for the day.

In the same way, the single-station indices ak and Ak are found from K by use of Table 4-4. In this form, these indices are normalized for station location (because K is),

Table 4-4. Value of ak for a given value of K.

If K =	0	1	2	3	4	5	6	7	8	9
then ak =	0	3	7	15	27	48	80	140	240	400

and comparison between stations is convenient. To remove the normalization, these indices are sometimes multiplied by a calibration factor f, given by $f = R_9/250$, where R_9 is the lower limit of R for K = 9. Indices so adjusted are quoted in units of nanoteslas. Thus at Fredericksburg, f = (500 nT)/250 = 2 nT. As an example of the complete circle, when R = 27 nT, K = 3, and ak = 15 (dimensionless) or ak = 30 nT.

The am index is similarly related to Km (there are also indices an and as corresponding to Kn and Ks), but in this case the a-type indices are derived directly from the data and the corresponding K-type index follows; that is, the awkward conversion-reconversion to and from a logarithmic scale is avoided. The am index is probably, in many respects, the best worldwide index currently available.

The aa index is similar to the am index but is derived from only two observatories situated at approximately antipodal locations in England and Australia. Although its development in the early 1970s was motivated by the availability of records from two old observatories (Greenwich and Melbourne) and has resulted in an index which spans 115 years (1868 to the present), it has also proved to be an

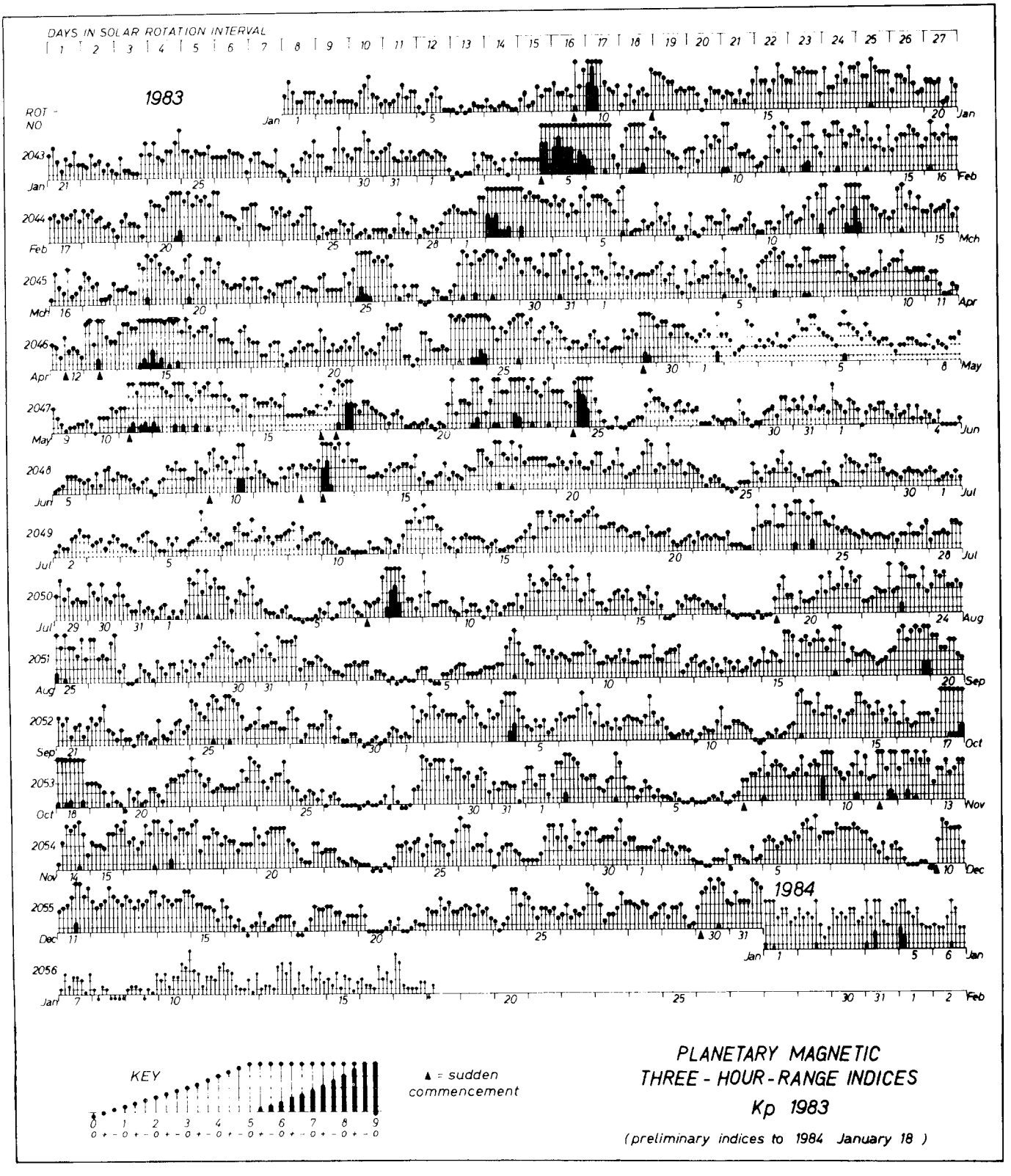

Figure 4-26. Musical-note diagram of Kp values for the year 1983, produced by the International Service of Geomagnetic Indices.

Table 4-5. Scale for finding Cp from the daily sum of ap. For each Cp interval the value listed is the upper limit of the daily-sum values in the interval.

If sum<	22	34	44	55	66	78	90	104	120	139	164	190	228
then Cp=	0.0	0.1	0.2	0.3	0.4	0.5	0.6	0.7	0.8	0.9	1.0	1.1	1.2
If sum<	273	320	379	453	561	729	1119	1399	1699	1999	2399	3199	—
then Cp=	1.3	1.4	1.5	1.6	1.7	1.8	1.9	2.0	2.1	2.2	2.3	2.4	2.5

easily obtainable but very good approximation to the am index.

4.7.3 Character Indices Cp, Ci, and C9

The Cp index, called the daily planetary character figure, is a number that ranges continuously from 0.0 to 2.5 and is quoted to tenths of an integer. It is found, using Table 4-5, from the daily sum (the sum of the eight 3-hour values) of the ap index. It restores the quasilogarithmic relationship originally introduced by the Kp scale and later removed by the ap scale. The peculiarity of its scale results from the intention that it should replace and be equivalent to a valuable older index, the Ci index, called the international daily character figure, available for all days since 1884. Cp is more reliable and objective, but usually differs from Ci by less than 0.2. Ci is obtained for each Greenwich day as the arithmetic mean of the C index values from a number of observatories; at each observatory the C index, called the daily magnetic character index, is reported as 0, 1, or 2 according to whether the UT day is quiet, moderately disturbed, or highly disturbed, respectively.

The C9 index, which can be found from Cp or Ci by use of Table 4-6, is sometimes used in their place especially for graphing, since it uses the more convenient single-digit zero-to-nine scale. Figure 4-27 shows a standard plot of the C9 index that, like the Kp musical-note diagram, shows recurrent 27-day activity.

4.7.4 Auroral-Electrojet Indices AE, AU, AL, and Ao

The AE index called the auroral electrojet activity index is derived from magnetograms from a number of auroral-zone stations distributed in longitude. It is intended to measure the strength of the auroral electrojet tabulated for hourly and (to some extent) 2.5-minute intervals. Obtained graphically from a single combined plot of the deviations at all stations of the element H from its normal quiet-time value, AE is the height of the envelope (that is, the difference) between the curves AU and AL (for "upper" and "lower") drawn through the maximum and minimum excursions of the deviations, respectively. The values of AU and AL are also used as indices, and another index Ao is defined to be the mean deviation, the curve midway between AU and AL.

4.7.5 Ring-Current Index Dst

The most widely used and available index of low-latitude activity is the hourly Dst index. It is the magnitude of the normalized horizontal component of the Dst field (axially symmetric disturbance), as determined from the data obtained by four low-latitude observatories distributed in longitude. The Dst index was designed as a measure of the magnetospheric ring current of magnetic storms; therefore, high-latitude and equatorial stations are avoided to minimize the effects of auroral and equatorial electrojets. The derivation was described by Sugiura [1964], who since the IGY has been the principal source of this index.

4.7.6 Other Indices

The Q index is an index which provides better time resolution than those based on the 3-hour K indices, but its availability is limited. It is a measure of high-latitude magnetic activity for each 15-minute interval, assigned by a number of observatories above 58 degrees geomagnetic latitude. It is computed, from the more disturbed of the elements X and Y, as the sum S of the absolute values of the maximum positive and maximum negative deviations from the normal (quiet) curve, with the provision that if the "negative" ("positive") deviation does not indeed become negative (positive), it is considered to be zero. The conversion

Table 4-6. Scale for finding C9 from Cp or Ci.

If Cp or Ci =	0.0 or 0.1	0.2 or 0.3	0.4 or 0.5	0.6 or 0.7	0.8 or 0.9	1.0 or 1.1	1.2 thru 1.4	1.5 thru 1.8	1.9	2.0 thru 2.5
then C9 =	0	1	2	3	4	5	6	7	8	9

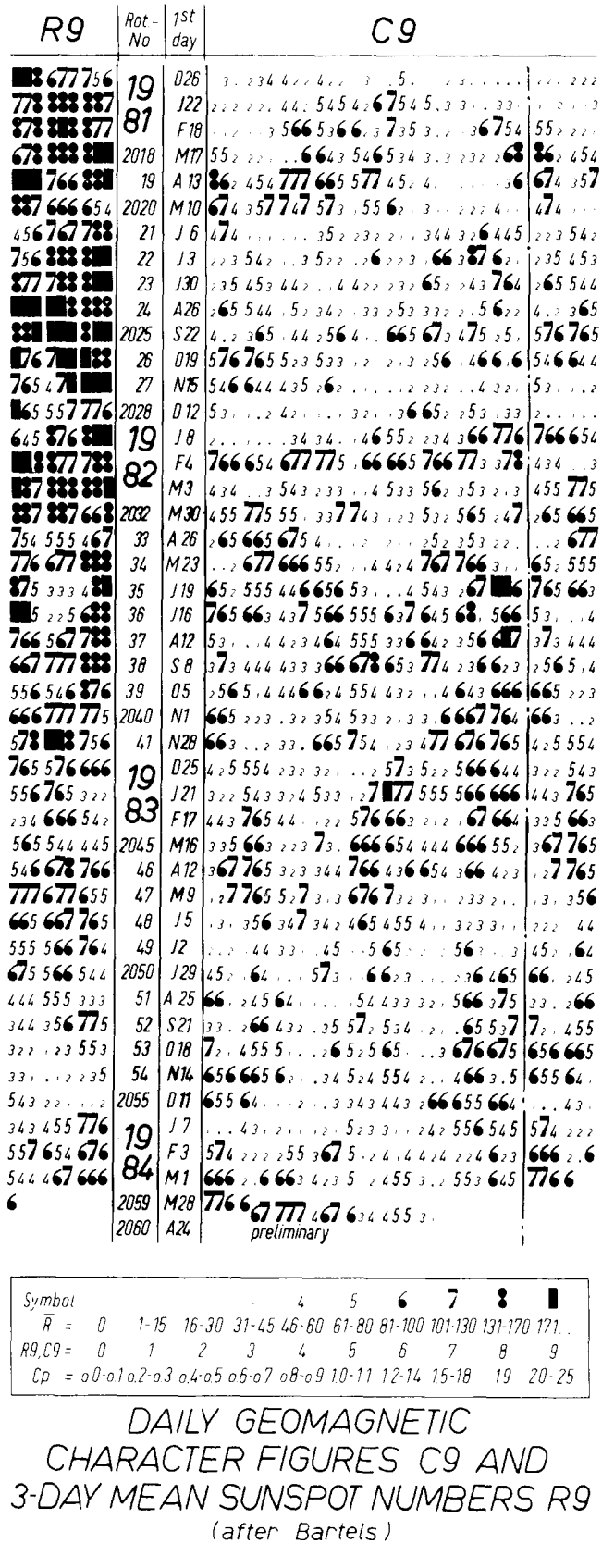

Figure 4-27. Plot of the C9 index and sunspot number R9 for the period 1981–1984.

scale for obtaining Q from S, applicable to all stations, is given in Table 4-7.

The indices U, u, u_1, and Δ are all derived from the difference between consecutive daily means of some element of the field. The U figure is the absolute magnitude of the difference between the daily means of the horizontal component for the given and preceding days. The u figure is a reduction of U to an equivalent equatorial value by the relation $u = U/(\sin \theta_m \cos \psi)$, where θ_m is geomagnetic colatitude and ψ is the angle between H and the magnetic meridian. The u_1 figure is obtained from u by a nonlinear conversion intended to reduce the influence of large disturbances. These indices have been useful historically for monthly and annual changes, but since they were intended to measure ring-current effects, the Dst index has largely superseded them.

The W measure applies to quiet variation fields rather than disturbance phenomena, being derived from the amplitude of the Sq variation. It is a measure of solar radiation effects and the intensity of the equatorial electrojet [Bartels, 1946].

4.8 SOURCES OF GEOMAGNETIC DATA

The following paragraphs provide some specific information on the availability of geomagnetic data. In recent years, the increasing emphasis on global studies of magnetospheric phenomena and the correlation of satellite and ground-based measurements have encouraged the extensive collection of such data at several data centers where they are made readily available. For data that are not archived there, the centers can often provide a referral to an alternative source.

4.8.1 Data Centers

Two national data centers in the United States have extensive holdings of geomagnetic data. The National Geophysical Data Center (NGDC) is operated by NOAA (Environmental Data and Information Service, NOAA, D63, 325 Broadway, Boulder, CO 80303, phone 303-497-6323). The NGDC is a recent successor to the National Geophysical and Solar-Terrestrial Data Center (NGSDC) and also serves internationally as the World Data Center A for Solar-Terrestrial Physics (WDC-A for STP). The National Space Science Data Center (NSSDC) is operated by NASA (Goddard Space Flight Center, Code 601, Greenbelt, MD 20771, phone 301-344-6695) and also serves as the World Data Center A for Rockets and Satellites. NGDC has magnetograms (as plots and computer tapes) and magnetic indices (in tabular, computer tape, and chart form). Both centers have space measurements (mostly nonduplicative) of mag

Table 4-7. Scale for finding Q from S. The listed value of S (in nT) is the upper limit for the corresponding value of Q.

If S <	10	20	40	80	140	240	400	660	1000	1500	2000	—
then Q =	0	1	2	3	4	5	6	7	8	9	10	11

netospheric magnetic fields, electric fields, and ULF/VLF phenomena. Both centers issue catalogs of their holdings and publications [Allen et al., 1982; National Space Science Data Center, 1981 and 1982].

Subcenters of the World Data Centers are also relevant to geomagnetism. They are organized into WDC-A (subcenters in the United States, including the two mentioned above), WDC-B (subcenters in the USSR, including one for solar-terrestrial physics at IZMIRAN, Moscow), and WDC-C (twenty subcenters in Europe, Japan, and India). WDC-A for STP now includes in its catalog the geomagnetic holdings of WDC-B2 (Moscow) and WDC-C2 (Kyoto).

4.8.2 International Organizations

The International Council of Scientific Unions (ICSU) includes 18 unions, which are nongovernmental organizations dedicated to scientific progress in various disciplines. Geomagnetism is a concern of the International Union of Geodesy and Geophysics (IUGG), which in the past has initiated such international collaborations as the International Geophysical Year and the International Magnetospheric Study. Within the IUGG a number of associations have been formed; geomagnetism falls within the concerns of the International Association of Geomagnetism and Aeronomy (IAGA). This association was originally the Section de Magnetisme et Electricite Terrestres (1919) and later the International Association of Terrestrial Magnetism and Electricity (1930) before taking its present name in 1954.

The IAGA has historically been a principal source of publications of geomagnetic data, including its Bulletins 12 series (covering 1940 through 1969) and Bulletins 32 series (covering 1970 through the present) of geomagnetic data, indices, rapid variations, and special intervals. The International Service of Geomagnetic Indices (ISGI) operates under supervision of the IAGA. Its services include the regular distribution of the Kp and C9 tables and charts from its Göttingen office (Institut für Geophysik, 34 Göttingen, W. Germany). Publications of both the IAGA and the ISGI are available from the IUGG Publications Office (39 ter rue Gay-Lussac, 75005 Paris, France). A catalog is available.

4.8.3 Magnetic Stations

Nearly 400 magnetic stations, data from which are held in the World Data Centers, are listed in Table 4-8, which is a condensation (omitting two sets of corrected coordinates) of Table II of the WDC-A catalog. Stations are listed in order of increasing uncorrected geomagnetic colatitude.

4.8.4 Magnetic Field Models

A number of magnetic-field models and computer programs for their use are now available from the National Space Science Data Center [see NSSDC, 1981, p. 55]. For many uses where the highest precision is not required hard-copy charts and tables may be more convenient. The IGRF 1975.0 field is available in this form. Barraclough and Fabiano [1977] present 14 charts (elements X, Y, Z, H, D, I, F and the secular variation in terms of their first time derivatives) and tables which list values for every five degrees of longitude and every two degrees of latitude. Publications resulting from the most current work with MAGSAT and other data can be expected from cooperative efforts at both NASA and the United States Geological Survey [Langel, 1980].

4.8.5 Activity Indices and Charts

At present, an excellent collection of indices has been assembled at the NGDC (Section 4.8.1). The widely used tables and charts furnished by the ISGI, as well as the publications of the IAGA, may be obtained through the IUGG Publications Office (see Section 4.8.2). A variety of sources current through 1971 was listed by Knecht [1972].

The periods for which various indices have been computed and published vary greatly, often depending on the resources available to the workers who have the capability. Even some of the currently most useful indices, such as AE and Dst, have been delayed. An enquiry as to the current coverage of any index (beyond that listed in the catalog) may be directed to the NGDC.

ACKNOWLEDGMENTS

The section on magnetic pulsations was written by H.J. Singer. Reference materials, recent data, and/or helpful comment were generously provided by R.H. Langel, J.C. Cain, and N.W. Peddie on current magnetic-field models; S. Matsushita on recent work on the Sq variation; T. Saito on the classification of pulsations; and J.H. Allen on the activities and holdings of the WDC-A for STP. The authors are very grateful for these contributions.

Table 4-8. List of geomagnetic stations from which the WDC-A has data holdings, listed in order of increasing geomagnetic colatitude. Successive columns are observatory name, international three-letter code, and uncorrected geomagnetic colatitude and east longitude.

THULE	THL	1.23	12.66	BIG DELTA	BDE	25.43	260.96	SEDDIN	SED	37.87	98.11
THULE AFB	THU	2.16	9.81	NORTHWAY	NRW	25.62	265.52	GOTTINGEN	GTT	37.99	94.82
ALERT	ALE	4.02	165.17	MALIYE KARMAKULY	MKL	25.62	143.82	NIEMEGK	NGK	38.01	97.67
RESOLUTE BAY	RES	6.82	292.87	MELVILLE AFB	MEV	25.63	13.72	DOURBES	DOU	38.30	88.88
NORTH POLE 7	NPG	6.91	195.37	KOTZEBUE	KOT	25.99	243.55	MANHAY	MAB	38.32	90.04
NORD	NRD	9.24	132.89	ISLAND LAKE	ISL	26.16	326.66	CASPER	CSR	38.42	316.25
GODHAVN	GDH	10.45	34.63	HEALY	HEA	26.19	258.17	MINSK	MNK	38.70	111.42
MOULD BAY	MBC	10.59	258.34	SODANKYLA	SOD	26.39	120.77	UGUT	UGT	38.72	153.19
PELLY BAY	PEB	11.37	322.55	BELLY ISLAND	BEY	26.40	155.68	COLLMBERG	CLL	38.78	97.61
GUANGZHOU	GZH	11.92	183.85	NORWAY HOUSE	NHO	26.42	322.51	YAKUTSK	YAK	38.79	194.94
GJOAHAVN	GJO	12.13	311.67	MURMANSK	MMK	26.65	126.55	VAL JOYEUX	VLJ	39.01	85.70
JOHNSON POINT	JOP	12.93	272.79	CAPE SCHMIDT	CPS	26.89	228.72	MAGADAN	MGD	39.02	211.57
CAMBRIDGE BAY	CBB	13.18	297.31	DIXON ISLAND	DIK	26.90	162.32	UKHTA	UKH	39.21	153.04
ARCTIC ICE FLO	AIF	13.64	208.33	LOVOZERO	LOZ	27.21	127.74	P. TUNGUSKA	POD	39.23	165.40
SUKKERTOPPEN	SKT	14.17	30.74	KANDALAKSHA	KND	27.56	125.02	MOSCOW	MOS	39.28	121.51
MURCHISON BAY	MUB	14.57	139.00	LERWICK	LER	27.75	89.64	SWIDER	SWI	39.61	105.69
SCORESBYSUND	SCO	14.60	82.63	TALKEETNA	TLK	27.81	258.60	BELSK	BEL	39.80	105.13
SACHS HARBOUR	SAH	14.60	267.47	CAPE WELLEN	CWE	27.87	238.48	NANTES	NTS	39.82	81.39
NEW AALESUND	NAL	14.69	131.33	DOMBAS	DOB	27.99	101.05	CHAMBON-LA-FORET	CLF	39.83	85.58
KAP TOBIN	KTG	15.26	274.22	MEANOOK	MEA	28.03	302.97	ANDREWS AFB	AWS	39.95	352.15
SPITZBERGEN	SPB	15.44	131.69	KHARASAVEY	KHS	28.21	152.32	CHELTENHAM	CLH	40.06	352.24
CAPE PARRY	CPY	16.00	271.96	TAMBEY	TMB	28.28	155.77	PRUHONICE	PRU	40.36	98.43
BAKER LAKE	BLC	16.17	317.73	ANCHORAGE	AMU	28.78	259.73	CARROLLTON	CAX	40.39	332.14
CHESTERFIELD INL	CFI	16.49	326.72	AMDERMA	AMD	29.27	147.69	FREDERICKSBURG	FRD	40.58	351.58
NORTH POLE 6	NPF	17.17	174.54	TIXIE BAY	TIK	29.33	192.38	BELOIT	BLT	40.75	326.63
RANKIN INLET	RIT	17.19	324.72	SEYKHA	SEY	29.69	155.52	KAZAN	KZN	40.76	131.37
NORTH POLE 12	NPL	17.38	218.58	SITKA	SIT	29.75	277.08	BOULDER	BOU	40.96	318.24
NORTH POLE 13	NPM	18.00	204.63	WHITESHELL	WHS	30.29	327.44	BUDKOV	BDV	41.12	97.51
TIKHAYA BAY	TKH	18.48	153.60	WINNIPEG	WNP	30.61	325.12	BALDWIN	BAL	41.14	330.25
HEISS ISLAND	HIS	18.64	156.47	GLENLEA	GLL	30.61	325.16	BURLINGTON	BRT	41.41	321.97
NORTH POLE 8	NPH	18.68	223.65	ARKHANGELSK	ARK	31.16	129.25	FURSTENFELDBRUCK	FUR	41.45	94.48
IVIGTUT	IVI	18.78	34.54	CAPE KAMENNIY	CKA	31.34	155.54	ARTI	ARS	41.52	139.57
BEAR ISLAND	BJN	19.00	124.95	NORILSK	NOK	31.40	165.68	SVERDLOVSK	SVD	41.54	141.70
ESKIMO POINT	EKP	19.03	323.51	LORING AFB	LOR	31.77	2.97	CLIMAX	CLI	41.83	317.35
NARSSARSSUAQ	NAQ	19.22	38.70	ST JOHNS	STJ	31.77	22.95	LEADVILLE	LDV	41.93	317.26
INUVIK	INK	19.29	267.10	ENKOPING	ENK	31.77	106.22	CHATONNAYE	CTE	42.01	89.50
JULIANEHAAB	JUL	19.49	37.24	ESKDALEMUIR	ESK	31.83	84.05	TEVRIZ	TEV	42.02	150.97
BARTER ISLAND	BTI	19.71	254.77	LOVO	LOV	32.15	106.77	LVOV	LVV	42.19	106.96
LEIRVOGUR	LRV	20.10	72.19	NURMIJARVI	NUR	32.32	113.53	PRICE	PCU	42.23	312.07
NORMAN WELLS	NOW	20.67	279.83	NYDA	NDA	33.14	154.34	WIEN-KOBENZL	WIK	42.33	99.34
FORT RAE	FRA	20.81	292.95	OTTAWA	OTT	33.34	353.43	KIEV	KIV	42.62	113.25
YELLOWKNIFE	YKC	20.84	295.38	STONYHURST	STO	33.36	83.87	NAGYCENK	NCK	43.02	99.44
BARROW	BRW	21.12	242.60	VALENTIA	VAL	33.68	74.70	ADAK	ADA	43.04	241.60
FORT CHURCHILL	FCC	21.28	325.00	LENINGRAD	LNN	33.92	118.29	HURBANOVO	HRB	43.08	100.92
NORTH POLE 10	NPJ	21.37	211.09	SLUTZK	SLU	34.15	117.94	O GYALLA	OGY	43.08	100.92
ARCTIC VILLAGE	AVI	21.77	256.17	RUDE SKOV	RSV	34.39	99.58	BUDAKESZI	BUZ	43.55	101.45
BACK	BKC	22.39	325.46	COPENHAGEN	COP	34.58	99.60	TIHANY	THY	43.95	100.25
BODO	BOD	22.56	113.41	NEWPORT	NEW	34.78	301.85	TOMSK	TMK	44.04	160.64
FORT SIMPSON	FSP	22.71	288.15	AGINCOURT	AGN	35.07	348.84	TULSA	TUL	44.06	330.06
CAPE ZHELANIA	CZA	22.77	157.59	VICTORIA	VIC	35.63	294.73	LOGRONO	LGR	44.25	78.46
TROMSO	TRO	23.04	117.42	HARTLAND	HAD	35.69	80.20	MONTE CAPELLINO	MCP	44.46	90.71
FORT YUKON	FYU	23.07	258.45	WINGST	WNG	35.71	95.15	GENOVA	GEN	44.46	90.71
GILLAM	GIM	23.22	325.64	WILHELMSHAVEN	WLH	35.75	94.14	ROBURENT	ROB	44.49	89.56
BOSSEKOP	BOP	23.52	121.06	NUMTO	NMT	36.03	152.03	CASTELLACCIO	CAO	44.57	90.64
GREAT WHALE R.	GWC	23.54	349.46	GREENWICH	GRW	36.08	85.02	SAO MIGUEL	SMG	44.70	52.30
CAPE CHELYUSKIN	CCS	23.57	177.18	WITTEVEEN	WIT	36.12	92.32	PETROPAVLOVSK	PET	45.02	219.87
LYNN LAKE	LYN	24.04	316.80	ABINGER	ABN	36.29	84.47	POLA	POL	45.11	95.59
ARISKO	ARK	24.17	115.70	WESTON	WES	36.30	358.86	COIMBRA	COI	45.29	71.55
THOMPSON	TMP	24.73	321.60	DE BILT	DBN	36.51	90.48	ESPANOLA	EPN	45.32	318.33
KIRUNA	KIR	24.91	116.38	SREDNIKAN	SRE	36.63	211.76	NOVOSIBIRSK	NVS	45.33	158.78
FORT SMITH	FSM	24.92	299.87	HEL	HLP	36.79	104.74	CASTLE ROCK	CRC	46.36	300.28
COLLEGE	CMO	25.06	258.14	KALININGRAD	KNG	37.04	106.43	EBRO	EBR	46.41	80.91
EIELSON AFB	ENB	25.09	259.03	BOROK	BOX	37.12	124.15	TOLEDO	TOL	46.44	75.95
PETSAMO	PTS	25.21	126.47	BOCHUM	BOC	37.50	92.15	ODESSA	ODE	46.51	112.23
IVALO	IVA	25.43	122.68	POTSDAM	POT	37.79	98.21	GROCKA	GCK	46.69	102.08

Table 4-8. *(Continued)*

DALLAS	DAL	47.05	329.44	FUQUENE	FUQ	73.23	356.55	PORT MORESBY	PMG	108.28	219.30
L AQUILA	AQU	47.41	94.14	PARAMARIBO	PAB	73.27	15.79	TSUMEB	TSU	108.46	84.24
SURLARI	SUA	47.68	107.22	FREETOWN	FTN	75.54	59.15	PILAR	PIL	110.42	5.93
LA MADDALENA	LMD	47.75	89.92	LUNPING	LNP	76.11	190.80	TANANARIVE	TAN	113.89	113.96
MT WILSON	MWC	48.64	305.48	UJJAIN	UJJ	76.51	148.22	LAS ACACIAS	LAS	113.93	11.39
SIMFEROPOL	SIM	48.97	114.45	ZARIA	ZAR	76.73	80.47	MAURITIUS	MRI	116.75	123.98
IRKUTSK	IRT	49.01	175.69	KONTAGORA	KNT	77.05	78.15	PLAISANCE	PLS	117.11	124.04
SAN FERNANDO	SFS	49.34	72.64	WAKE ISLAND	WKE	77.18	234.42	MAPUTO	LMM	117.92	97.31
CAPRI	CPI	49.35	94.38	CHA PA	CPA	78.92	174.57	TRELEW	TRW	121.97	4.37
PANAGYURISHTE	PAG	49.37	104.54	HONG KONG	HKC	79.09	184.35	CAPE GOOD HOPE	CGH	122.97	81.41
TUCSON	TUC	49.49	313.84	KUMASI	KUM	79.35	70.46	CAPE TOWN	CTO	122.99	81.39
KARAGANDA	KGD	49.66	149.76	IBADAN	IBD	79.66	76.03	HERMANUS	HER	123.59	81.99
ALMERIA	ALM	49.68	76.58	TATUOCA	TTB	80.70	22.19	BRISBANE	BRS	125.44	228.32
ISTANBUL-KANDILL	ISK	51.70	108.63	ALIBAG	ABG	80.76	144.58	WATHEROO	WAT	131.54	187.28
KHABAROVSK	KHB	51.92	201.24	HYDERABAD	HYB	82.35	150.24	MAGALLANES	MGS	131.88	359.61
AVERROES	AVE	52.20	70.45	TALARA	TAL	83.51	349.08	GNANGARA	GNA	133.02	187.40
NOVOKAZALINSK	NKK	52.41	139.55	EUSEBIO	EUS	84.27	32.09	CANBERRA	CAN	133.66	225.74
YUZHNO SAKHALINS	YSS	52.82	207.92	PALMYRA ISLAND	PAI	84.56	267.21	SOUTH GEORGIA	SGE	134.51	27.19
ULAN BATOR	UBA	53.46	177.63	MOCA	MFP	84.58	79.94	TOOLANGI	TOO	136.34	222.32
TBILISI	TFS	53.47	123.24	BAGUIO	BAG	84.70	190.60	AMBERLEY	AML	137.34	253.80
PENDELI	PEG	53.64	102.81	ADDIS ABABA	AAE	84.82	110.51	EYREWELL	EYR	137.67	253.52
KZIL-AGACH	KZA	54.59	153.76	BANGUI	BNG	85.46	89.87	CHRISTCHURCH	CHR	137.72	253.84
CANARIAS	TEN	55.34	59.99	CHICLAYO	CCL	85.63	350.65	MARION ISLAND	MRN	139.24	95.90
SANTA CRUZ	SZT	55.34	59.99	GUAM	GUA	85.73	214.26	LAUDER	LAU	139.72	251.36
MEMAMBETSU	MMB	55.70	209.70	FANNING	FAN	85.97	270.24	ORCADAS DEL SUR	ORC	140.25	19.31
HAVANA	HVN	55.97	346.94	ANTIPOLO	ANO	86.50	191.22	PORT ALFRED	CZT	141.51	110.57
ALMA ATA	AAA	56.53	151.88	MANILA	MAN	86.53	191.04	GONZALES VIDELA	GVD	143.57	5.41
VLADIVOSTOK	VLA	56.90	199.36	MUNTINLUPA	MUT	86.73	191.09	ARGENTINE ISLAND	AIA	143.93	4.35
TASHKENT	TKT	57.68	145.19	BANGKOK	BKK	87.46	171.23	CAMPBELL ISLAND	CAI	146.97	254.44
ASHKHABAD	ASH	59.56	134.30	CHIMBOTE	CMB	87.89	351.91	PORT-AUX-FRANCAI	KGL	147.43	129.83
KSARA	KSA	60.00	112.96	MAJURO	MJR	88.35	241.03	MACQUARIE ISLAND	MCQ	150.75	244.41
TEOLOYUCAN	TEO	60.44	328.62	ANNAMALAINAGAR	ANN	88.61	150.45	HEARD ISLAND	HIT	151.48	131.91
VIEQUES	VQS	60.58	5.41	KODAIKANAL	KOD	89.40	148.45	SANAE	SNA	153.95	45.40
SAN JUAN	SJG	60.59	4.65	JARVIS ISLAND	JRV	90.30	270.45	EIGHTS	EGS	153.96	256.08
TEHRAN	TEH	60.75	127.73	ETTAYAPURAM	ETT	90.67	148.84	NORWAY STATION	NWS	154.11	45.09
MIZUSAWA	MIZ	60.84	207.69	CEBU	CCP	90.68	194.08	LAZAREV	LZV	155.98	56.69
BEIJING	BJI	61.23	185.75	HUANCAYO	HUA	90.77	355.19	HALLEY BAY	HBA	156.06	25.25
ONAGAWA	ONW	61.39	208.12	TRIVANDRUM	TRD	91.08	147.75	NOVOLAZAREVSKAYA	NVL	156.51	54.94
MODIIM	MOD	61.71	111.65	CUZCO	CUS	92.21	358.48	ROI BAUDOUIN	RBD	158.33	64.67
NITSANIM	NSM	61.81	111.24	MOGADISCIO	MOG	92.90	115.68	SYOWA STATION	SYO	159.96	79.38
AMATSIA	AMT	62.04	111.49	KOROR	KOR	92.95	204.73	MOLODEZHNAYA	MOL	159.97	07.36
HELWAN	HLW	63.02	107.69	BINZA	BIN	93.45	84.91	BYRD STATION	BYR	160.62	336.71
MISALLAT	MLT	63.28	107.20	DAVAO	DAV	93.81	195.90	MAWSON	MAW	163.31	105.08
KAKIOKA	KAK	63.69	207.25	LWIRO	LWI	94.01	98.60	LITTLE AMERICA	LAA	163.95	312.23
TOKYO	TOK	64.21	206.90	YAUCA	YAU	94.24	355.88	LENINGRADSKAYA	LEN	164.33	261.97
KANOZAN	KNZ	64.68	207.19	NAIROBI	NAI	94.63	106.67	CAPE HALLETT	HLL	164.47	278.80
TAMANRASSET	TAM	64.92	80.88	CHARACATO	ARE	95.15	358.97	DUMONT DURVILLE	DRV	165.33	232.38
MIYAZU	MIU	65.02	202.83	LA PAZ	LPB	95.19	2.22	MIRNY	MIR	167.02	149.66
LANZHOU	LZH	65.17	174.87	PENANG	PNN	95.68	170.81	OASIS	OAS	167.37	163.53
MIDWAY	MDY	65.59	247.75	LUANDA	LUA	97.49	81.96	PLATEAU	PTU	167.53	53.79
SIMOSATO	SSO	66.69	203.74	DAR ES SALAAM	DRS	100.44	108.00	WILKES	WIL	167.57	181.85
HACHIJO	HJJ	66.81	207.29	LA QUIACA	LQA	100.82	4.54	CHARCOT	CTX	167.94	235.93
HATIZYO	HTY	66.86	207.32	VASSOURAS	VSS	102.22	25.21	SOUTH POLE	SPA	168.68	0.00
ASO	ASO	67.74	199.36	HOLLANDIA	HNA	102.25	211.70	SCOTT BASE	SBA	168.80	294.35
QUETTA	QUE	68.40	140.97	RIO DE JANEIRO	RDJ	102.77	25.60	MCMURDO	MCM	168.82	294.31
HONOLULU	HON	68.64	267.97	SAN JOSE	SJB	102.86	23.07	PIONERSKAYA	PIO	170.33	149.88
M BOUR	MBO	69.08	56.40	ELIZABETHVILLE	ELI	102.94	95.37	VOSTOK	VOS	179.41	111.76
COSTA RICA	SNJ	69.09	345.69	KARAVIA	KVA	102.94	95.37				
KANOYA	KNY	69.20	199.36	TAHITI	TAH	105.11	284.04				
SABHAWALA	SAB	69.44	150.95	PAMATAI	PPT	105.12	284.09				
LUKIAPANG	LKP	69.80	190.40	APIA	API	105.75	261.58				
ZIKAWEI	ZKW	69.88	190.77	KUYPER	KUY	107.34	177.02				
SHESHAN	SSH	70.01	190.55	TANGERANG	TNG	107.47	176.91				
CHICHIJIMA	CBI	72.57	210.19	BATAVIA	BTV	107.49	177.12				
JAIPUR	JAI	72.63	148.68	EASTER ISLAND	EIC	108.18	323.88				

CHAPTER 4

REFERENCES

Alldredge, L.R. and L. Hurwitz, "Radial Dipoles as the Sources of the Earth's Main Magnetic field," *J. Geophys. Res.*, **69:** 2631, 1964.

Allen, J.H., C.C. Abston, Z.R. Kharin, and N. Papitashvili, International Catalog of Geomagnetic Data, *Report UAG-86,* World Data Center A for Solar-Terrestrial Physics, Boulder, CO, 1982.

Axford, W.I., "Tail of the Magnetosphere," *J. Geophys. Res.*, **70:** 1231, 1965.

Barraclough, D.R. and E.B. Fabiano (eds) Grid Values and Charts for the IGRF 1975.0. *IAGA Bulletin No. 38,* 1977. (Available not from IUGG but as NTIS No. PB-276 63s.)

Bartels, J., "Geomagnetic Data on Variations of Solar Radiation: Part I—Wave Radiation," *Terr. Magn. Atmos. Elec.*, **5:** 181, 1946.

Bullard, E.C., C. Freedman, H. Gellman, and J. Nixon, "The Westward Drift of the Earth's Magnetic Field," *Phil. Trans. Roy. Soc.*, **243A:** 67, 1950.

Chapman, S. and J. Bartels, *Geomagnetism,* Oxford University Press, London, 1940.

Chen, L. and A. Hasegawa, "A Theory of Long-Period Magnetic Pulsations, 1, Steady State Excitation of Field Line Resonance," *J. Geophys. Res.*, **79:** 1024, 1974.

Cummings, W.D., R.J. O'Sullivan, and P.J. Coleman, Jr., "Standing Alfvén Waves in the Magnetosphere," *J. Geophys. Res.*, **74:** 778, 1969.

Dungey, J.W., "Electrodynamics of the Outer Atmosphere," *Sci. Rep. 69,* Ionos. Res. Lab., Pennsylvania State University, 1954. (Also partially contained in Dungey, J.W., "The Structure of the Exosphere, or Adventures in Velocity Space," *Geophysics: The Earth's Environment,* edited by DeWitt, Hieblot and Lebeau, Gordon and Breach, New York, 1963).

Greenwald, R.A. and A.D.M. Walker, "Energetics of Long Period Resonant Hydromagnetic Waves," *Geophys. Res. Lett.*, **7:** 745, 1980.

Gustafsson, G., "A Revised Corrected Geomagnetic Coordinate System," *Ark. Geofys.*, **5:** 595, 1970.

Hakura, Y., "Tables and Maps of Geomagnetic Coordinates Corrected by the Higher Order Spherical Harmonic Terms," *Rep. Ionosph. Space Res. Japan,* **19:** 121, 1965.

Hughes, W.J., "Pulsation Research During the IMS," *Rev. Geophys. Space Phys.*, **20:** 641, 1982.

Hughes, W.J., "Hydromagnetic Waves in the Magnetosphere", submitted to U.S. National Report to 18th General Assembly of IUGG Hamburg, Aug. 1983.

IAGA Division 1 Working Group 1, International Geomagnetic Reference Fields: DGRF 1965, DGRF 1970, DGRF 1975, and IGRF 1980, *Eos Trans AGU* **62:** 1169, 1981.

IAGA, "Review Papers from the ULF Symposium held at the 4th IAGA Scientific Assembly, Edinburgh, 14 August 1981," *Planet. Space Sci.*, **30:** 1199–1258, 1982.

Jacobs, J.A., *Geomagnetic Micropulsations,* Springer-Verlag, New York, 1970.

Knecht, D.J., "The Geomagnetic Field," *AFCRL-72-0570,* AD 759837, 1972.

Langel, R.A., "Magsat Scientific Investigations" *NASA Technical Memorandum 80698,* May, 1980.

Langel, R.A., private communication, 1982.

Lanzerotti, L.J. and D.J. Southwood, "Hydromagnetic Waves," in *Solar System Plasma Physics,* III, 109, edited by E.N. Parker, C.F. Kennel, L.J. Lanzerotti, North Holland, Amsterdam, 1979.

Matsushita, S., "Solar Quiet and Lunar Daily Variation Fields," in *Physics of Geomagnetic Phenomena*, edited by S. Matsushita and W.H. Campbell, Academic Press, New York, 1967.

Matsushita, S., "Morphology of Slowly Varying Geomagnetic External Fields—A Review," *Phys. Earth Plan. Int.*, **10:** 299, 1975.

Matsushita, S. and H. Maeda, "On the Geomagnetic Solar Quiet Daily Variation Field During the IGY," *J. Geophys. Res.*, **70:** 2535, 1965a.

Matsushita, S. and H. Maeda, "On the Geomagnetic Lunar Daily Variation Field," *J. Geophys. Res.*, **70:** 2559, 1965b.

Mayaud, P.N., *Derivation, Meaning, and Use of Geomagnetic Indices,* (Geophysical Monograph 22) AGU, Washington, D.C., 1980.

Nagata, T., "Two Main Aspects of Geomagnetic Secular Variation—Westward Drift and Nondrifting Components" in *Benedum Earth Magnetism Symposium* edited by T. Nagata, University of Pittsburgh Press, 1962.

Nagata, T. and M. Ozima, "Paleomagnetism," in *Physics of Geomagnetic Phenomena* edited by S. Matsushita and W.H. Campbell, Academic Press, New York, 1967.

National Space Science Data Center, NSSDC Data Listing, *NSSDC Report 81-11,* Goddard Space Flight Center, Greenbelt, Md., September 1981.

National Space Science Data Center, Data Catalog Series for Space Science and Applications Flight Missions, *NSSDC Report 82-21* (Vol. 1A) and *NSSDC Report 82-22* (Vol. 2A), Goddard Space Flight Center, Greenbelt, Md., September 1982.

Nishida, A., *Geomagnetic Diagnosis of the Magnetosphere,* Springer-Verlag, New York, 1978.

Olson, W.P. and K.A. Pfitzer, "A Quantitative Model of the Magnetospheric Magnetic Field," *J. Geophys. Res.*, **79:** 3739, 1974.

Olson, W.P., and K.A. Pfitzer, "Magnetospheric Magnetic Field Modeling," McDonnell-Douglas Astronautics Co. Rept, 1977.

Orr, D., "Magnetic Pulsations Within the Magnetosphere: A Review," *J. Atmos. Terr. Phys.*, **35:** 1, 1973.

Orr, D., (ed.), "Geomagnetic Pulsations: Papers from 7th Annual E.G.S. Meeting," *J. Atmos. Terr. Phys.*, **43**(9): 1981.

Parkinson, W.D. and J. Cleary, "The Eccentric Geomagnetic Dipole," *Geophys. J. Roy. Astron. Soc.*, **1:** 346, 1958.

Saito, T., "Geomagnetic Pulsations," *Space Sci. Rev.*, **10:** 319, 1969.

Saito, T., "Long-period Irregular Magnetic Pulsations, Pi 3," *Space Sci. Rev.*, **21:** 427, 1978.

Shawhan, S.D., "Magnetospheric Plasma Wave Research 1975–1978," *Rev. Geophys. Space Phys.*, **17:** 705, 1979.

Singer, H.J., "Multisatellite Observations of Resonant Hydromagnetic Waves," *Planet. Space Sci.*, **30:** 1209, 1982.

Singer, H.J., D.J. Southwood, R.J. Walker, and M.G. Kivelson, "Alfvén Wave Resonances in a Realistic Magnetospheric Magnetic Field Geometry," *J. Geophys. Res.*, **86:** 4589, 1981.

Southwood, D.J., "Some Features of Field Line Resonances in the Magnetosphere," *Planet. Space Sci.*, **22:** 483, 1974.

Southwood, D.J., "Waves, Wave Particle Interactions and Magnetic Oscillations," *IAGA Report*, International Association of Geomagnetism and Aeronomy, Dec. 1979.

Southwood, D.J. (ed.), "ULF Pulsations in the Magnetosphere," *J. Geomagn. Geoelec.*, **32,** Suppl. II, 1980.

Southwood, D.J. and W.J. Hughes, "Theory of Hydromagnetic Waves in the Magnetosphere," *Space Sci. Rev.*, **35:** 301, 1983.

Southwood, D.J. and W.F. Stuart, "Pulsations at the Substorm Onset," *Dynamics of the Magnetosphere*, edited by S.-I. Akasofu, D. Reidel, Dordrecht, Holland 1980.

Sugiura, M., "Hourly Values of Equatorial Dst for the IGY," *Annals of the Int. Geophys. Year*, **35:** 49, 1964.

Tsyganenko, H.A., "A Model of the Cis-Lunar Magnetospheric Field," *Ann. Geophys.*, **32:** 1, 1976.

Vestine, E.H., "Influence of the Earth's Core upon the Rate of the Earth's Rotation," in *Benedum Earth Magnetism Symposium*, edited by T. Nagata, University of Pittsburgh Press, Pittsburgh, 1962.